Cell

NLRP6 Inflammasome Regulates Colonic Microbial Ecology and Risk for Colitis

Eran Elinav,[1,8] Till Strowig,[1,8] Andrew L. Kau,[4,5] Jorge Henao-Mejia,[1] Christoph A. Thaiss,[1] Carmen J. Booth,[2] David R. Peaper,[3] John Bertin,[6] Stephanie C. Eisenbarth,[1,3] Jeffrey I. Gordon,[4] and Richard A. Flavell[1,7,*]

[1]Department of Immunobiology
[2]Section of Comparative Medicine
[3]Department of Laboratory Medicine
Yale University School of Medicine, New Haven, CT 06520, USA
[4]Center for Genome Sciences and Systems Biology
[5]Division of Allergy and Immunology, Department of Internal Medicine
Washington University School of Medicine, Saint Louis, MO 63108, USA
[6]Pattern Recognition Receptor Discovery Performance Unit, GlaxoSmithKline, Collegeville, PA 19426, USA
[7]Howard Hughes Medical Institute, Chevy Chase, MD 20815, USA
[8]These authors contributed equally to this work
*Correspondence: richard.flavell@yale.edu
DOI 10.1016/j.cell.2011.04.022

SUMMARY

Inflammasomes are multiprotein complexes that function as sensors of endogenous or exogenous damage-associated molecular patterns. Here, we show that deficiency of NLRP6 in mouse colonic epithelial cells results in reduced IL-18 levels and altered fecal microbiota characterized by expanded representation of the bacterial phyla Bacteroidetes (*Prevotellaceae*) and TM7. NLRP6 inflammasome-deficient mice were characterized by spontaneous intestinal hyperplasia, inflammatory cell recruitment, and exacerbation of chemical colitis induced by exposure to dextran sodium sulfate (DSS). Cross-fostering and cohousing experiments revealed that the colitogenic activity of this microbiota is transferable to neonatal or adult wild-type mice, leading to exacerbation of DSS colitis via induction of the cytokine, CCL5. Antibiotic treatment and electron microscopy studies further supported the role of *Prevotellaceae* as a key representative of this microbiota-associated phenotype. Altogether, perturbations in this inflammasome pathway, including NLRP6, ASC, caspase-1, and IL-18, may constitute a predisposing or initiating event in some cases of human IBD.

INTRODUCTION

The distal intestine of humans contains tens of trillions of microbes; this community (microbiota) is dominated by members of the domain Bacteria but also includes members of Archaea and Eukarya and their viruses. The vast repertoire of microbial genes (microbiome) that are present in the distal gut microbiota performs myriad functions that benefit the host (Qin et al., 2010). The mucosal immune system coevolves with the microbiota beginning at birth, acquiring the capacity to tolerate components of the microbial community while maintaining the capacity to respond to invading pathogens. The gut epithelium and its overlying mucus provide a physical barrier. Epithelial cell lineages, notably the Paneth cell, sense bacterial products through receptors for microbe-associated molecular patterns (MAMPs), resulting in regulated production of bactericidal molecules (Vaishnava et al., 2008). Mononuclear phagocytes continuously survey luminal contents and participate in maintenance of tissue integrity and the initiation of immune responses (Macpherson and Uhr, 2004; Niess et al., 2005; Rescigno et al., 2001).

Several families of innate receptors expressed by hematopoietic and nonhematopoietic cells are involved in recognition of MAMPs, such as Toll-like receptors (TLRs), nucleotide-binding oligomerization domain protein-like receptors (NLRs), and C-type lectin receptors (Geijtenbeek et al., 2004; Janeway and Medzhitov, 2002; Martinon et al., 2002). Inflammasomes are cytoplasmic multiprotein complexes that are composed of one of several NLR proteins, including NLRP1, NLRP3, and NLRC4, which function as sensors of endogenous or exogenous stress or damage-associated molecular patterns (Schroder and Tschopp, 2010). Upon sensing the relevant signal, they assemble, typically together with the adaptor protein, apoptosis-associated speck-like protein (ASC), into a multiprotein complex that governs caspase-1 activation and subsequent cleavage of effector proinflammatory cytokines, including pro-IL-1β and pro-IL-18 (Agostini et al., 2004; Martinon et al., 2002).

Several other members of the NLR family, including NLRP6 and NLRP12, possess the structural motifs of molecular sensors and are recruited to the "specks" formed in the cytosol by ASC oligomerization, leading to procaspase-1 activation (Grenier

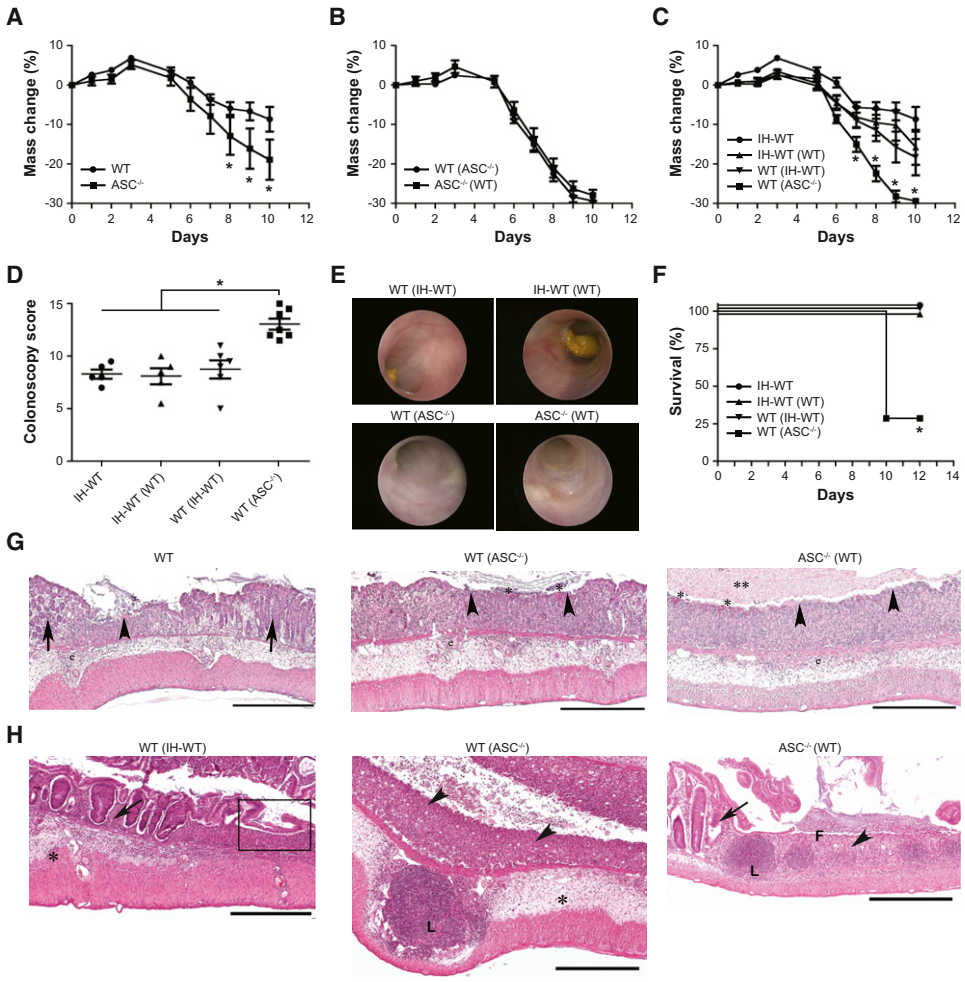

Figure 1. The Increased Severity of Colitis in ASC-Deficient Mice Is Transmissible to Cohoused Wild-Type Mice

(A and B) To induce colitis, mice were given 2% DSS in their drinking water for 7 days. (A) Weight loss of *ASC*$^{-/-}$ mice and separately housed wild-type (WT) mice. (B) *ASC*$^{-/-}$ mice and WT mice were cohoused for 4 weeks, after which DSS colitis was induced.

(C–F) Weight loss (C), colonoscopy severity score at day 7 (D), and survival (F) after induction of DSS colitis of WT mice that were cohoused with (i) in-house WT mice bred for several generations in our vivarium (IH-WT) or (ii) *ASC*$^{-/-}$ mice (designated WT(IH-WT) and WT(*ASC*$^{-/-}$), respectively). (E) Representative images taken during colonoscopy of mice at day 7.

(G and H) Representative H&E-stained sections of colons from WT(IH-WT), WT(*ASC*$^{-/-}$), and *ASC*$^{-/-}$(WT) mice sampled on day 6 (G) and day 12 (H) after the start of DSS exposure. Epithelial ulceration (arrowheads), severe edema/inflammation (asterisk) with large lymphoid nodules (L), retention/regeneration of crypts (arrows), and evidence of re-epithelialization/repair of the epithelium (box).

Scale bars, 500 μm. Data are representative for three independent experiments. Error bars represent the SEM of samples within a group. *p < 0.05 by one-way ANOVA. For related data, see Figures S1A–S1D.

et al., 2002; Wang et al., 2002). However, the triggers and function of NLRP12 are only now being revealed (Arthur et al., 2010), and those of NLRP6 remain unknown. In this study, we describe a mechanism for how the immune system regulates colonic microbiota via an inflammasome that requires NLRP6, ASC, and caspase-1 and leads to the cleavage of pro-IL-18. In mice that are deficient in NLRP6, ASC, caspase-1, or IL-18, gut microbial ecology is altered, with prominent changes in the representation of members of several bacterial phyla. Strikingly, this altered microbiota is associated with a colitogenic phenotype that is transmissible to cohoused wild-type mice, both early in postnatal life and during adulthood.

RESULTS

ASC-Deficient Mice Develop Severe DSS Colitis that Is Transferable to Cohoused WT Mice

To characterize possible links between inflammasome function and homeostasis achieved between the innate immune system and the gut microbiota, we studied mice that are deficient in ASC. A more severe colitis developed after dextran sodium sulfate (DSS) administration to single-housed *ASC*$^{-/-}$ mice than in wild-type (WT) mice purchased from a commercial vendor (National Cancer Institute, NCI) (Figure 1A and data not shown). Remarkably, cohousing of adult *ASC*$^{-/-}$ mice with age-matched

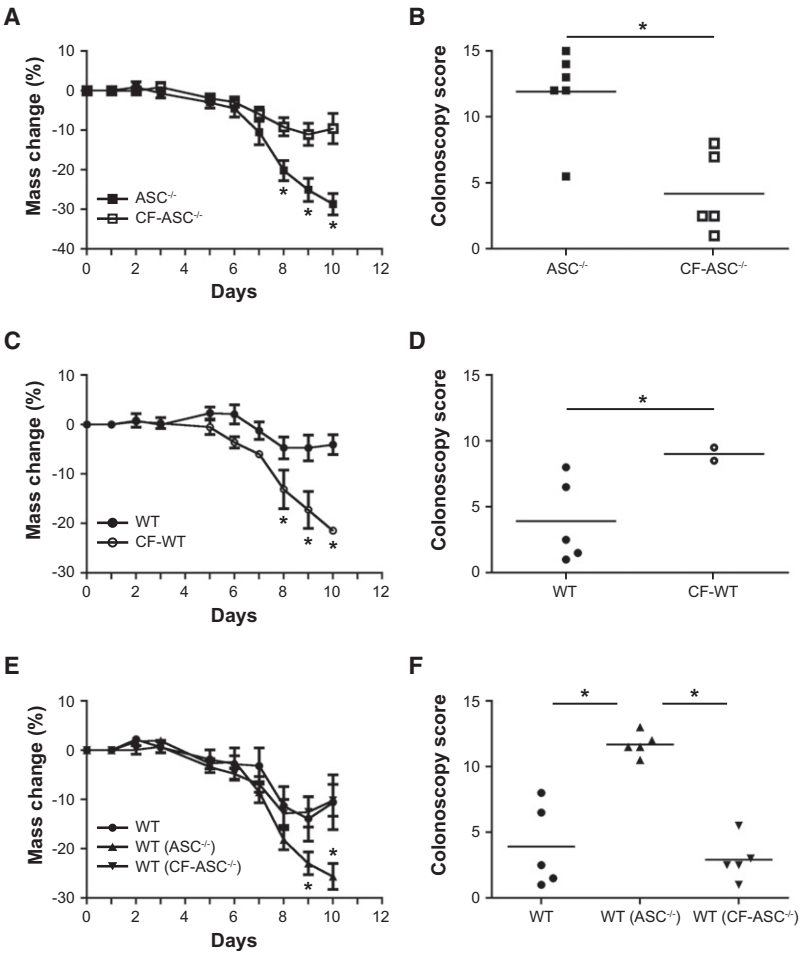

Figure 2. Maternal Transmission of an Exacerbated DSS Colitis Phenotype

(A–F) Newborn *ASC*$^{-/-}$ and WT mice were swapped between their respective mothers (cross-fostered), followed by induction of acute DSS colitis at 8 weeks of age. Body weight and colonoscopy severity score were measured in *ASC*$^{-/-}$ mice and *ASC*$^{-/-}$ mice cross-fostered with WT mothers (CF-*ASC*$^{-/-}$) (A and B); WT mice and WT mice cross-fostered with *ASC*$^{-/-}$ mothers (CF-WT) (C and D); WT mice cohoused with *ASC*$^{-/-}$ or cross-fostered *ASC*$^{-/-}$ mice for 4 weeks (E and F). Data are representative of three independent experiments. Error bars represent the SEM of samples within a group. *$p < 0.05$ by one-way ANOVA. Figures S1E–S1G contain related data.

WT mice for 4 weeks prior to induction of DSS colitis resulted in development of comparably severe DSS-induced colitis in *ASC*$^{-/-}$ as well as cohoused WT mice (the latter are designated "WT(*ASC*$^{-/-}$)" in Figure 1B).

To assess the possibility that differences in colitis severity observed between groups of single-housed *ASC*$^{-/-}$ and WT mice were indeed driven by differences in their intestinal microbiota, WT mice were cohoused for 4 weeks with either *ASC*$^{-/-}$ mice (WT(*ASC*$^{-/-}$)) or WT mice that had been bred in our vivarium for more than ten generations (in-house mice (IH-WT), WT(IH-WT)). The severity of DSS-induced colitis was similar among NCI-WT (data not shown), IH-WT, and WT(IH-WT) as well as IH-WT(WT) as judged by weight loss (Figure 1C), colitis severity score (defined by colonoscopy) (Figures 1D and 1E), and survival (Figure 1F). In contrast, WT(*ASC*$^{-/-}$) and *ASC*$^{-/-}$ mice were characterized by an equally increased severity of disease compared to these other groups at both early and late stages (Figures 1C–1H and Figures S1A–S1D available online).

To further establish the role of the intestinal microbiota, we performed cross-fostering experiments. Newborn *ASC*$^{-/-}$ mice cross-fostered (CF) at birth with in-house WT mothers (CF-*ASC*$^{-/-}$) exhibited milder colitis compared to noncross-fostered *ASC*$^{-/-}$ mice (Figures 2A and 2B). In contrast, newborn WT mice cross-fostered with *ASC*$^{-/-}$ mothers (CF-WT) developed severe colitis in comparison to noncross-fostered WT mice (Figures 2C and 2D). Moreover, CF-*ASC*$^{-/-}$ mice were no longer able to transmit enhanced colitis to cohoused WT mice (Figures 2E and 2F).

Separation of cohoused WT mice from *ASC*$^{-/-}$ mice and subsequent housing with naive WT mice resulted in a gradual partial reduction in colitis severity compared to WT(*ASC*$^{-/-}$) mice that were not exposed to a WT microbiota (Figures S1E–S1G). Together, these results demonstrate that the *ASC*$^{-/-}$ microbiota is a dominant colitogenic factor, transmissible early in life to WT mice, and that this colitogenic activity is sustainable in recipient mice for prolonged periods of time. Nonetheless, exposure of an established transferred *ASC*$^{-/-}$-derived microbiota in a WT mouse to WT microbiota ameliorates its colitogenic potential, suggesting that the latter community can displace the former and diminish its disease-promoting properties in WT mice.

Culture-independent methods were subsequently employed to compare the gut microbial communities. PCR was used to amplify variable region 2 (V2) of bacterial 16S rRNA genes present in fecal samples collected from *ASC*$^{-/-}$ and WT mice just prior to and 28 days following cohousing. The amplicons generated were subjected to multiplex pyrosequencing, and the resulting chimera-checked and filtered data sets were compared using UniFrac (mean of 3524 ± 1023 [SD] 16S rRNA reads/sample; see Experimental Procedures for details). Figure 3A shows a clear difference in fecal bacterial phylogenetic architecture in WT versus *ASC*$^{-/-}$ mice. Moreover, after 4 weeks of cohousing, the fecal bacterial communities of WT(*ASC*$^{-/-}$) mice clustered together with communities from their *ASC*$^{-/-}$ cagemates. In addition, the bacterial component of the fecal microbiota of these cohoused *ASC*$^{-/-}$ mice was similar to *ASC*$^{-/-}$ mice that never had been cohoused.

NLRP6-Deficiency Produces a Microbiota-Mediated Phenotype that Resembles that of ASC Deficiency

To assess whether ASC's function as adaptor protein for inflammasome formation is linked to the changes in gut bacterial

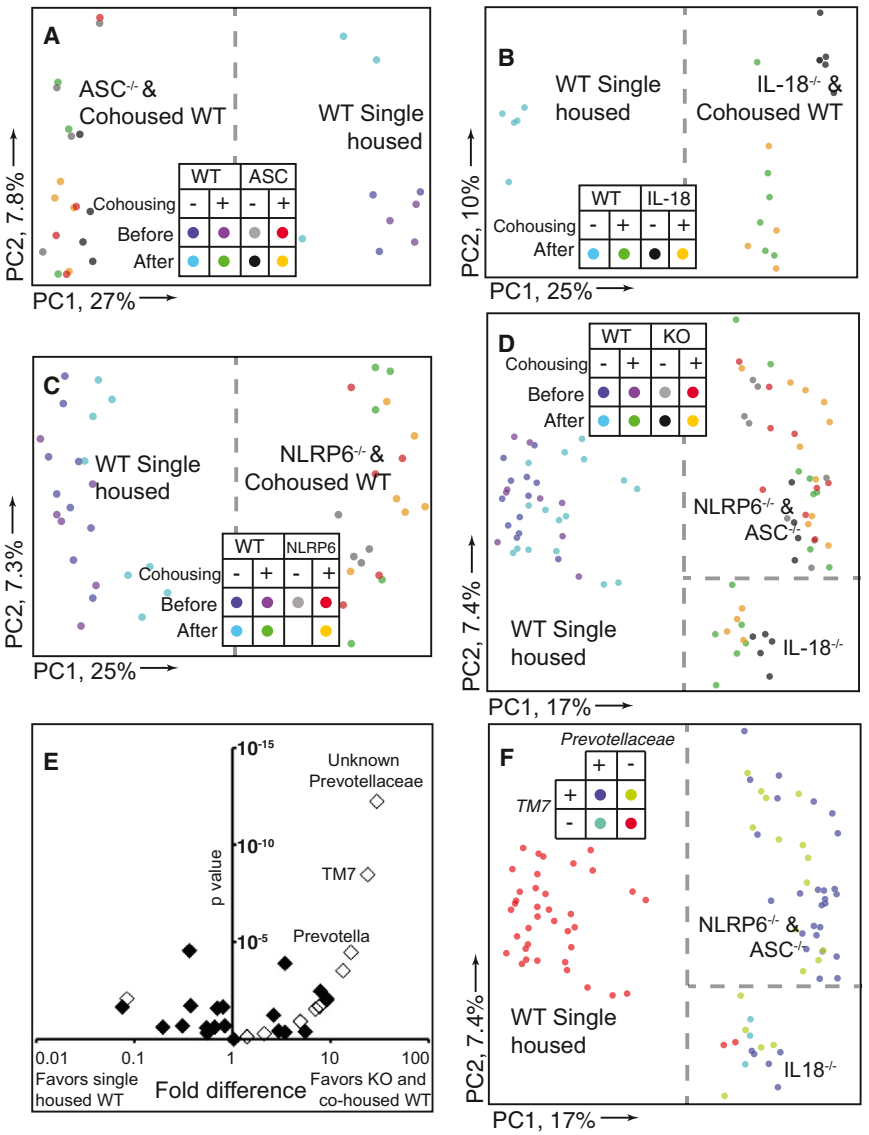

Figure 3. Bacterial 16S rRNA-Based Analysis of the Fecal Microbiota of WT and *NLRP6* Inflammasome-Deficient Mice

(A–D) Unweighted UniFrac PCoA of fecal microbiota harvested from WT mice single-housed or cohoused with *ASC*$^{-/-}$ (A), *IL-18*$^{-/-}$ (B), *NLRP6*$^{-/-}$ (C), or all (D) mice. Samples from mice shown in (A) and (C) were taken just prior to cohousing and 28 days later. Dashed line illustrates separation of samples along PC1.

(E) Distribution of family-level phylotypes in ASC-, IL-18-, NLRP6-deficient, and cohoused WT mice, compared to single-housed WT mice. The horizontal axis shows the fold representation (defined as the ratio of the percentage of samples with genera present in knockout or cohoused mice versus single-housed WT mice). The left side of the axis indicates taxa whose representation is greater in single-housed WT mice; the right denotes taxa whose representation is greater in knockout or cohoused WT mice. The origin represents equivalent recovery of taxa in both groups. The vertical axis shows the calculated p value for each taxa as defined by G test. Open diamonds represent taxa that were found only in KO/cohoused WT or single-housed WT mice but where recovery was assumed to be 1 to calculate fold representation.

(F) Unweighted UniFrac PCoA demonstrating presence or absence of TM7 and *Prevotellaceae* in each sample. Dashed lines show separation of single-housed WT and cohoused WT and knockout mice on PC1. PC2 in panels (D) and (F) shows separation of communities based on host genotype/cohousing. For additional data related to the transmission of fecal microbiota in inflammasome deficient mice, see Figure S2.

community structure and function observed, we cohoused WT mice with *caspase-1*$^{-/-}$ mice, and these too exhibited more severe DSS-induced colitis compared to single-housed WT mice (Figures S2A–S2E). Similar to WT mice cohoused with *ASC*$^{-/-}$ mice, WT mice cohoused with *caspase-1*$^{-/-}$ mice evolved their intestinal bacterial communities to a phylogenetic configuration that was very similar to that of their *caspase-1*$^{-/-}$ cagemates (Figure S2F). These results point to the involvement of an inflammasome in this phenotype.

We next sought to identify the NLR(s) upstream of ASC and caspase-1 leading to the phenotype. qRT-PCR analysis of 24 tissues in WT mice revealed that NLRP6, which forms an ASC-dependent inflammasome (Grenier et al., 2002), is most highly expressed in the gastrointestinal tract and at lower levels in lung, kidney, and liver (Figure 4A). Further, we isolated RNA prepared from colonic epithelium and sorted colonic CD45^{+} hematopoietic cells and found that ASC and caspase-1 are highly expressed in both compartments. NLRP6 expression, in contrast, was essentially limited to the epithelial compartment (Figure 4B). Indeed, in bone marrow transfer experiments, NLRP6 was almost undetectable in *NLRP6*$^{-/-}$ mice (Figures S3A and S3B) receiving WT bone marrow (Figure 4C). Follow-up immunoprecipitation (Figure 4D) and immunofluorescence assays (Figures 4E and 4F) both showed that NLRP6 protein is expressed in primary colonic epithelial cells of WT mice, where it mainly appears within speckled cytoplasmic aggregates, whereas it was absent in *NLRP6*$^{-/-}$ mice.

WT and *NLRP6*$^{-/-}$ mice were then single housed or cohoused for 4 weeks, followed by exposure to DSS. Single-housed *NLRP6*$^{-/-}$ mice developed more severe colitis compared to single-housed WT mice (Figures 4G–4J). The more severe colitis phenotype was transferable to cohoused WT mice (WT(*NLRP6*$^{-/-}$)) (Figures 4G–4J and Figures S3C–S3G). 16S rRNA analysis of fecal bacterial communities demonstrated a clear difference in the bacterial community structure between single-housed adult WT mice versus age-matched WT mice cohoused for 4 weeks with NLRP6-deficient mice (Figure 3C). Fecal bacterial communities of WT mice clustered together

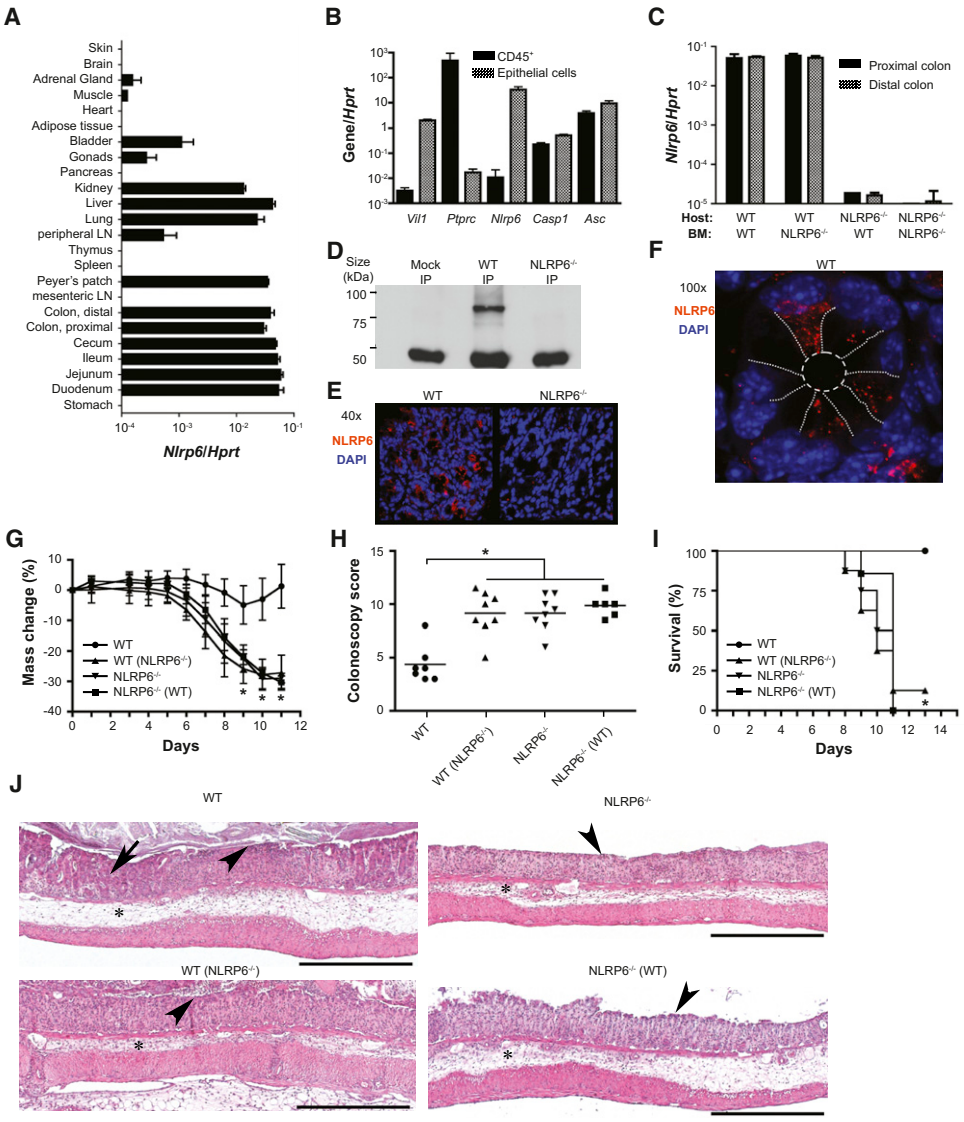

Figure 4. NLRP6-Deficient Mice Harbor a Transmissible Colitogenic Gut Microbiota

(A and B) (A) Analysis of NLRP6 expression in various organs and (B) in colonic epithelial and hematopoietic ($CD45^+$) cells. The purity of the sorted populations in (B) was analyzed using *vil1* and *ptprc* as markers for epithelial and hematopoietic cells, respectively.

(C) Bone marrow chimeras were generated using WT and *NLRP6*$^{-/-}$ mice as host and bone marrow donor. NLRP6 expression in the colon was analyzed 8 weeks after bone marrow transplantation.

(D) Analysis of NLRP6 protein expression was performed by immunoprecipitation using an NLRP6 antibody and lysates of primary colonic epithelial cells isolated from WT and *NLRP6*$^{-/-}$ mice.

(E and F) Representative confocal images of colonic sections analyzed for expression of NLRP6 (red) and counterstained with DAPI. (E) 40×, (F) 100×. White dotted lines were drawn to illustrate the epithelial cell boundaries.

(G–J) Acute DSS colitis was induced in single-housed WT mice, in WT mice cohoused for 4 weeks with *NLRP6*$^{-/-}$ mice (WT(*NLRP6*$^{-/-}$), the corresponding cohoused *NLRP6*$^{-/-}$ mice (*NLRP6*$^{-/-}$(WT)), and single-housed *NLRP6*$^{-/-}$ mice (*NLRP6*$^{-/-}$). Weight (G), colonoscopy severity score at day 8 (H), and survival (I) of single-housed versus cohoused WT and *NLRP6*$^{-/-}$ mice. (J) Representative H&E-stained sections of colons on day 7 after initiation of DSS exposure. Edema/inflammation (asterisks), ulceration (arrowheads), and loss of crypts (arrow). Scale bars, 500 μm. Data are representative of three independent experiments. Error bars represent the SEM of samples within a group. *$p < 0.05$ by one-way ANOVA. Related data are in Figure S3 and Table S1.

with communities from their *NLRP6*$^{-/-}$ cagemates whose microbiota in turn was similar to *NLRP6*$^{-/-}$ mice that never had been cohoused (Figure 3C).

To ascertain the specificity of this phenotype, we cohoused WT mice with mice that lacked other NLR family members and inflammasome-forming protein AIM2, all shown by qRT-PCR analysis to be expressed in the colon (Figure S4A) (Kufer and Sansonetti, 2011; Schroder and Tschopp, 2010). Adult, conventionally raised, specific pathogen-free knockout mice were either obtained from the same source as *NLRP6*$^{-/-}$ mice (Millenium,

NLRP3$^{-/-}$, *NLRC4*$^{-/-}$, *NLRP12*$^{-/-}$), generated in our own laboratory (*NLRP10*$^{-/-}$), or obtained from other laboratories (*AIM2*$^{-/-}$, K Fitzgerald, U. Massachusetts). *NLRP3*$^{-/-}$ mice cohoused with WT mice for 4 weeks featured attenuated colitis as compared to their WT cagemates and mild transferability of colitis, suggesting that NLRP3's major effect in this system is negative regulation of the inflammatory process itself (data not shown). Importantly, none of the other above mentioned mouse strains transferred microbiota with increased colitogenic properties to WT mice upon cohousing (Figures S4B–S4I). Likewise, 16S rRNA analysis of these strains revealed a distinct configuration of their microbiota population as compared to NLRP6 inflammasome-deficient mice (Table S1). Together, these findings indicate that NLRP6 forms an intestinal epithelial inflammasome that regulates functional properties of the microbiota and that loss of NLRP6 and the known inflammasome constituents, ASC and caspase-1, leads to the specific development of a transmissible, more colitogenic microbiota.

Evidence that NLRP6 Affects the Gut Microbiota via IL-18

Activation of inflammasomes results in multiple downstream effects, including proteolytic cleavage of pro-IL-1β and pro-IL-18 to their active forms (Schroder and Tschopp, 2010). To test whether the effect of NLRP6 deficiency is mediated via IL-1β or IL-18 deficiency, we cohoused adult WT mice with either *IL-1β*$^{-/-}$ (Figure 5A) or *IL-1R*$^{-/-}$ mice (Figures S4J and S4K). Cohousing WT mice with these strains did not result in any significant changes in the severity of DSS colitis compared to single-housed WT mice, excluding a major contribution of the IL-1 axis. In contrast, *IL-18*$^{-/-}$ mice and, more importantly, WT mice cohoused with them exhibited a significant exacerbation of colitis severity, compared to single-housed WT mice (Figures 5B–5F).

In the steady state, single-housed *NLRP6*$^{-/-}$ mice had significantly reduced serum levels of IL-18 compared to their WT counterparts and reduced production of this cytokine in their colonic explants (Figures 5G and 5H). To study the relative contribution of hematopoietic and nonhematopoietic NLRP6 deficiency to this reduction in active IL-18, we measured IL-18 protein levels in colonic explants prepared from chimeric mice that had received bone marrow transplants from *NLRP6*$^{-/-}$ or WT donors. Significantly lower IL-18 protein levels were noted only in explants prepared from mice with NLRP6 deficiency in the nonhematopoietic compartment (Figure 5I). This result indicates that NLRP6 expressed in a nonhematopoietic component of the colon, likely the epithelium, is a major contributor to production of active IL-18. Furthermore, in contrast to WT mice, *NLRP6*$^{-/-}$ mice failed to significantly upregulate IL-18 in the serum and in tissue explants following induction of DSS colitis (Figure 5J and data not shown).

To study whether IL-18 production by nonhematopoietic cells is the major contributor to the microbiota-associated enhanced colitogenic phenotype, we performed a bone marrow transfer experiment using *IL-18*$^{-/-}$ and WT mice as both recipients and donors. Indeed, mice that were deficient in IL-18 in the nonhematopoietic compartment exhibited more severe disease compared to mice that were sufficient for IL-18 in the nonhematopoietic compartment (Figures 5K and 5L). Bacterial 16S rDNA studies demonstrated that the fecal microbiota of WT mice exposed to *IL-18*$^{-/-}$ mice changed its phylogenetic configuration to resemble that of *IL-18*$^{-/-}$ cagemates (Figure 3B). Interestingly, as seen in the PC2 axis in the PCoA plot of unweighted UniFrac distances, the fecal microbiota of *ASC*$^{-/-}$ and *NLRP6*$^{-/-}$ mice were distinct from *IL-18*$^{-/-}$ mice, possibly reflecting the existence of additional NLRP6 inflammasome-mediated IL-18-independent mechanisms of microflora regulation (Figure 3D). Together, these results led us to conclude that the decrease in colonic epithelial IL-18 production in mice that are deficient in components of the NLRP6 inflammasome is critically involved in the enhanced colitogenic properties of the microbiota.

The Gut Microbiota from NLRP6 Inflammasome-Deficient Mice Induces CCL5 Production and Immune Cell Recruitment, Leading to Spontaneous Inflammation

We next examined the intestines of untreated *ASC*$^{-/-}$ and *NLRP6*$^{-/-}$ mice for signs of spontaneous pathological changes. The colons, terminal ileums, and Peyer's patches of *ASC*$^{-/-}$ and *NLRP6*$^{-/-}$ mice exhibited colonic crypt hyperplasia, changes in crypt-to-villus ratios in the terminal ileum, and enlargement of Peyer's patches with formation of germinal centers (Figure 6A and Figures S5A and S5B). NLRP6 inflammasome-deficient mice also had significantly elevated serum IgG2c and IgA levels, as did cohoused WT mice (Figures S5C–S5F). In addition, we recovered significantly more CD45^{+} cells from colons of *NLRP6*$^{-/-}$ mice compared to WT controls (Figure 6B). These results prompted us to investigate downstream effector mechanisms by which the altered microbiota could induce this immune cell infiltration. Multiplex analysis of cytokine and chemokine production by tissue explants (Figure S5G), followed by validation at the RNA (Figure 6C) and protein levels (Figure 6D), indicated that CCL5 levels were significantly elevated in single-caged untreated *ASC*$^{-/-}$, *NLRP6*$^{-/-}$, and *IL-18*$^{-/-}$ compared to WT mice. Furthermore, CCL5 mRNA upregulation was found to originate from epithelial cells (Figure 6E). Moreover, CCL5 levels were induced in WT mice upon cohousing (Figures 6F and 6G), showing that this property was specified by the microbiota and not the mutated inflammasome per se. Notably, in the steady state, *CCL5*$^{-/-}$ mice and WT mice featured a comparable representation of immune subsets with the exception of slight reduction in γδ TCR^{+} lymphocytes, indicating that CCL5 is not generally required for immune cell recruitment to the colon (Figure S5H).

To test the role of CCL5 in mediating the enhanced colitogenic properties of the *NLRP6*$^{-/-}$ mouse microbiota, we cohoused WT or *CCL5*$^{-/-}$ mice with *NLRP6*$^{-/-}$ mice for 4 weeks. We subsequently induced DSS colitis and found comparable colitis severity between single-housed WT and *CCL5*$^{-/-}$ mice (Figures 6H and 6I). However, upon cohousing, WT(*NLRP6*$^{-/-}$) mice had significantly worse DSS-induced colitis compared to *CCL5*$^{-/-}$(*NLRP6*$^{-/-}$) mice, despite comparable acquisition of the *NLRP6*$^{-/-}$ colitogenic flora (Figure S5I). These findings support the notion that CCL5 upregulation in response to the altered microbiota is responsible for the exacerbation of colitis that occurs in WT mice cohoused with NLRP6 inflammasome-deficient mice.

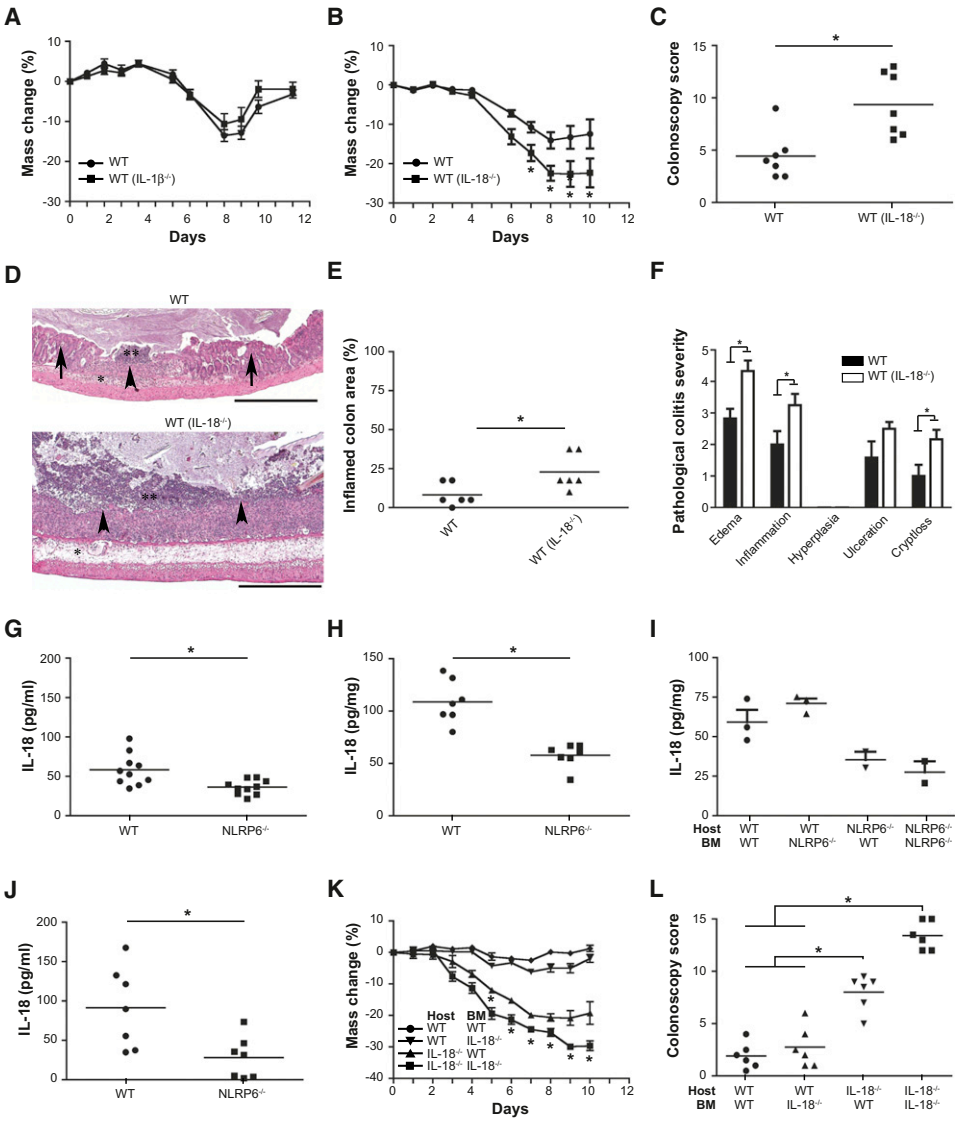

Figure 5. Processing of IL-18 by NLRP6 Inflammasome Suppresses Colitogenic Microbiota

(A–C) WT mice were cohoused with *IL-1β*$^{-/-}$ mice or *IL-18*$^{-/-}$ mice for 4 weeks, and colitis was subsequently induced with DSS. Comparison of weight loss (A) in single-housed WT mice and in WT mice previously cohoused with *IL-1β*$^{-/-}$ mice (WT(*IL-1β*$^{-/-}$)). Weight loss (B) and colonoscopy severity score at day 7 (C) for single-housed WT mice and WT mice previously cohoused with *IL-18*$^{-/-}$ mice (WT(*IL-18*$^{-/-}$)).

(D–F) Representative H&E-stained sections (D) and pathologic quantitation of disease severity (E and F) of colons from single-housed WT mice and WT mice cohoused with *IL18*$^{-/-}$ mice sampled 6 days after the start of DSS administration. Scale bars, 500 μm.

(G and H) IL-18 levels measured in sera (G) and colon explants (H) obtained from WT and NLRP6-deficient mice without treatment.

(I) Bone marrow chimeras were generated using both WT and *NLRP6*$^{-/-}$ mice as host and bone marrow donor. IL-18 production by colon explants was analyzed 8 weeks after bone marrow transplantation.

(J) IL-18 concentrations in the serum 5 days after induction of DSS colitis.

(K and L) Bone marrow chimeras were generated using WT and *IL-18*$^{-/-}$ mice as host and bone marrow donor. Weight (K) and colonoscopy severity scores at day 7 (L) of mice with acute DSS colitis are shown.

Data in (A–E) are representative of at least three experiments; data in (I–L) are representative of two experiments. n = 6 mice/samples analyzed per group. *$p < 0.05$ by one-way ANOVA. Related data are presented in Figure S4.

Identification of Bacterial Phylotypes that Are Markedly Expanded in Both NLRP6 Inflammasome-Deficient Mice and in Cohoused WT Mice

To identify whether increased colitis severity is driven by bacterial components, we first treated *ASC*$^{-/-}$ mice with a combination of antibiotics known to reduce the proportional representation of a broad range of bacterial phylotypes in the gut (Suzuki et al., 2004; Rakoff-Nahoum et al., 2004). Antibiotic therapy reduced the severity of DSS colitis in *ASC*$^{-/-}$ mice to WT levels (Figures S6A and S6B). To exclude a possible role for

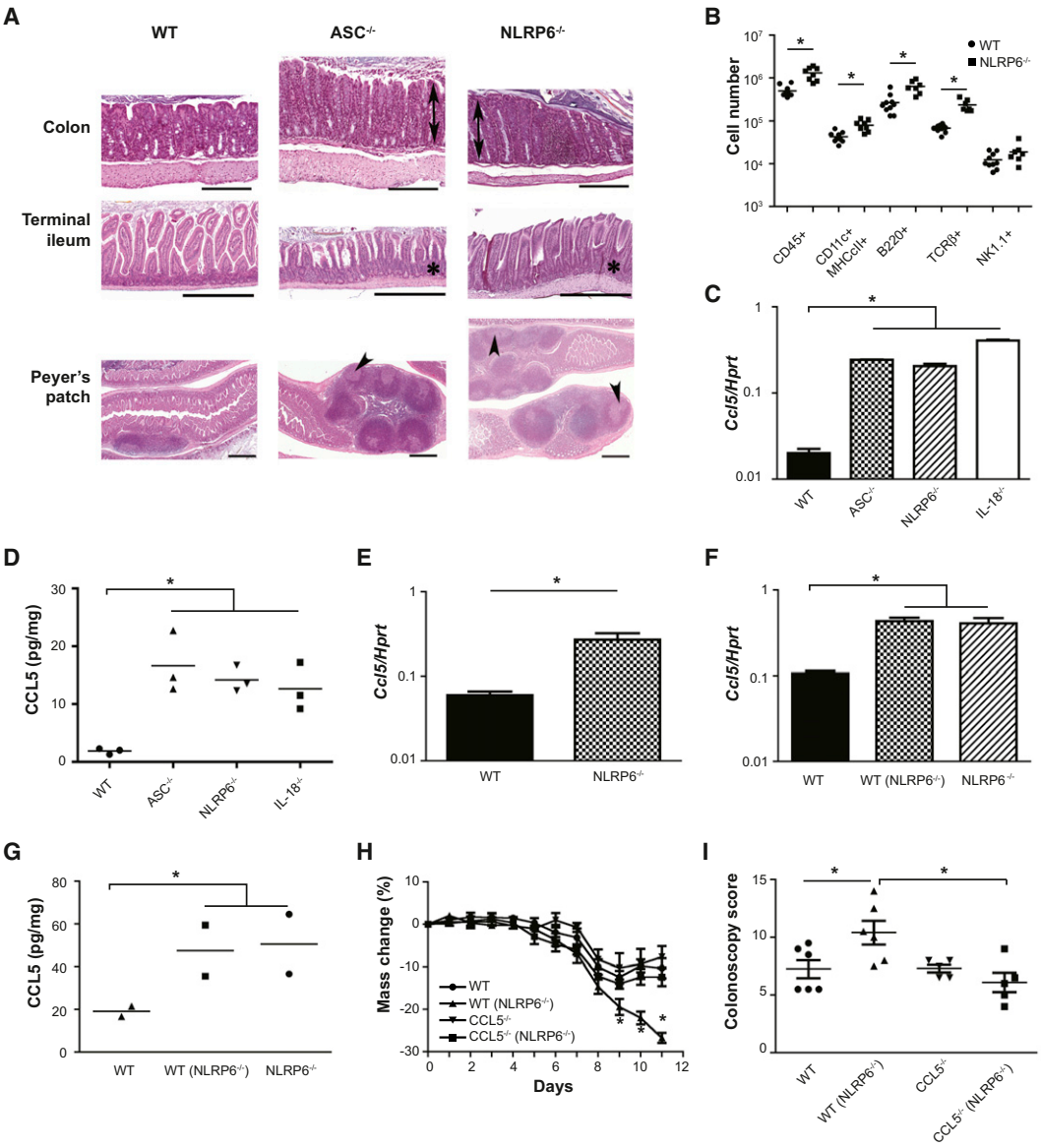

Figure 6. Microbiota Induction of CCL5

(A) Representative H&E-stained sections of the colon, terminal ileum, and Peyer's patches from WT, *ASC*$^{-/-}$, and *NLRP6*$^{-/-}$ mice not exposed to DSS. Mucosal hyperplasia in the colon (double arrows), increased crypt to villus ratio in the terminal ileum (asterisks), and enlargement of Peyer's patches with formation of germinal centers (arrowheads). Scale bars, 500 μm.

(B) Enumeration of subsets of hematopoietic cells harvested from the lamina propria of WT and *NLRP6*$^{-/-}$ mice.

(C and D) Analysis of CCL5 colonic mRNA expression (C) and protein expression in colonic explants (D) in WT, *ASC*$^{-/-}$, *NLRP6*$^{-/-}$, and *IL-18*$^{-/-}$ mice.

(E) CCL5 expression in epithelial cells from the colons of WT and *NLRP6*$^{-/-}$ mice.

(F and G) Analysis of CCL5 colonic mRNA expression (F) and protein expression in colonic explants (G) in single-housed WT mice and WT mice cohoused with *NLRP6*$^{-/-}$ mice.

(H and I) WT and *CCL5*$^{-/-}$ mice were either single-housed or cohoused for 4 weeks with *NLRP6*$^{-/-}$ mice followed by exposure to DSS. Weight loss (H) and colonoscopy severity score at day 7 (I) of mice after induction of acute DSS colitis.

Data shown in (A–G) are representative of at least two experiments. Data presented in (H) and (I) are from three experiments. n = 5–6 mice. Error bars represent the SEM of samples within a group. *p < 0.05 by one-way ANOVA. Additional cytokine and chemokine analyses are presented in Figure S5.

herpesviruses, fungi, and parasites, single-housed WT and *ASC*$^{-/-}$ mice were treated for 3 weeks with oral gancyclovir, amphotericin, or albendazole and praziquantel, respectively. None of these treatments altered the severity of colitis in ASC-deficient mice (Figures S6C–S6E). Furthermore, fecal tests for rotavirus, lymphocytic choriomeningitis virus, K87, murine cytomegalovirus, mouse hepatitis virus, mouse parvovirus, reovirus, and Theiler's murine encephalomyelitis virus were all negative,

and there was no histological evidence of inclusion bodies, which are characteristic of virally infected colonic epithelial cells (data not shown). Together, these results pointed to bacterial components as being responsible for the transferrable colitis phenotype in NLRP6 inflammasome-deficient mice.

Table S1 lists bacterial phylotypes whose presence or absence was significantly different in (i) single-housed WT mice compared to (ii) *ASC*$^{-/-}$ and *NLRP6*$^{-/-}$, and *caspase-1*$^{-/-}$, and *IL-18*$^{-/-}$, and all types of cohoused WT mice (all untreated with DSS). Nine genera belonging to four phyla (Firmicutes, Bacteroidetes, Proteobacteria, and TM7) satisfied our requirement of having significant differences in their representation in the fecal microbiota in group (i) versus group (ii). The genus-level phylotype that is most significantly associated with the fecal microbiota of *ASC*$^{-/-}$, *NLRP6*$^{-/-}$, *caspase-1*$^{-/-}$, *IL-18*$^{-/-}$, and cohoused WT mice was a member of the family *Prevotellaceae* in the phylum Bacteroidetes. Beyond this unnamed genus in the *Prevotellaceae*, the next two most discriminatory genus-level taxa belonged to the phylum TM7 and the named genus Prevotella within the *Prevotellaceae* (Figure 3E and Figure S2G). Likewise, *Prevotellaceae* was absent from single-housed *CCL5*$^{-/-}$ mice and highly acquired following cohousing with *NLRP6*$^{-/-}$ mice (Figures S5J and S5K). Also included in this list was a member of the family Helicobacteraceae (order Campylobacterales); tests for the pathogen *Helicobacter hepaticus* were consistently negative in these mice (n = 6 samples per strain screened with PCR).

Histopathologic analyses of colonic sections stained with hematoxylin and eosin as well as Warthin-Starry stain disclosed microbes with a long branching, striated morphotype that is closely associated with the crypt epithelium of single-housed *ASC*$^{-/-}$ and *NLRP6*$^{-/-}$ mice; these organisms were rare in WT mice (Figure S6F and data not shown). This morphotype is consistent with members of TM7 (Hugenholtz et al., 2001). Quadruple antibiotic treatment for 3 weeks eliminated microbes with this morphology from *ASC*$^{-/-}$ mice as judged by histopathologic analysis (n = 5 mice; data not shown).

A significant reduction in *Prevotellaceae* was noted in stools of *NLRP6*$^{-/-}$ mice that were treated with the same combination of four antibiotics. The most complete eradication was achieved using a combination of metronidazole and ciprofloxacin, a commonly used regimen for treatment of human IBD (Figure 7A). The severity of DSS colitis was also significantly reduced in antibiotic-treated compared to untreated *NLRP6*$^{-/-}$ mice (Figures 7B and 7C).

Next, we tested whether antibiotic treatment affected the ability of *NLRP6*$^{-/-}$ mice to transfer the colitogenic microbiota to WT mice. Strikingly, WT mice cohoused with antibiotic-treated *NLRP6*$^{-/-}$ mice developed significantly less-severe DSS colitis compared to WT mice cohoused with untreated *NLRP6*$^{-/-}$ mice (Figures 7D and 7E). This reduction in severity correlated with decreased abundance of *Prevotellaceae* and TM7, but not of *Bacteroidetes* in WT mice cohoused with antibiotic-treated *NLRP6*$^{-/-}$ mice (Figure 7F and Figures S6G and S6H). Low-level representation of *Prevotellaceae* was noted in nonphenotypic NLR-deficient mice bred for generations in our vivarium (Table S1). As representative NLRs, we decided to directly compare the quantitative differences in *Prevotellaceae* abundance and its impact on transmissibility to WT mice between *NLRP6*$^{-/-}$ and *NLRC4*$^{-/-}$ mice, as the latter lacks a closely related colonic-epithelium-expressed protein that is also able to form an inflammasome and process IL-18. Indeed, *NLRC4*$^{-/-}$ and their cohoused WT cagemates featured a clustering pattern in the PCoA plot (Figure 7G) distinct from both single-housed WT mice as well as from *NLRP6*$^{-/-}$ mice and cohoused WT mice. Specifically, *Prevotellaceae* was highly abundant in *NLRP6*$^{-/-}$ mice though low to absent in *NLRC4*$^{-/-}$ mice, their cohoused WT cagemates, and single-housed WT mice (Figure 7H).

To determine whether NLRP6 deficiency was associated with an alteration in the physical distribution (biogeography) of the microbiota within the gut, we analyzed colon tissue that had been thoroughly washed of fecal matter (see Experimental Procedures for details). This enabled enhanced detection of bacteria residing in crypts. TM7 and *Prevotellaceae* were significantly more prevalent in the washed colons of *NLRP6*$^{-/-}$ mice compared to WT and *NLRC4*$^{-/-}$ mice (Figure 7I and data not shown). Further, transmission electron microscopy studies revealed multiple monomorphic bacteria in crypt bases of *ASC*$^{-/-}$ and *NLRP6*$^{-/-}$, but not WT and *NLRPC4*$^{-/-}$ mice, featuring an abundance of electron dense intracellular material that is consistent with the pigmentation that is characteristic of many Prevotella species (Figures 7J–7L and data not shown). Overall, these findings indicate that the dysbiosis in NLRP6 inflammasome-deficient mice may involve aberrant host-microbial cross-talk within the colonic crypt.

DISCUSSION

We describe a regulatory sensing system in the colon that is dependent on the NLRP6 inflammasome. We show that genetic deletion of components of this sensing system has drastic consequences on the composition of the microbial communities, leading to a shift toward a proinflammatory configuration that drives spontaneous and induced colitis.

On a molecular level, it appears unlikely that the evolutionarily conserved, innate mucosal immune arm possesses the ability to distinctly identify the myriad bacterial, archaeal, and eukaryotic microbial phylotypes and virotypes that comprise the gut microbiota and differentiate autochthonous (entrenched) or allochthonous (transient/nomadic) components of this community that act as commensals or mutualists from those that act as pathogens. Rather, this function may be achieved by sensing signals that are related to tissue integrity or factors released by tissue damage that serve as "danger signals" promoting activation of an innate response (Matzinger, 2007). Inflammasomes are capable of fulfilling this task, as they can be activated by many microbial ligands, but also by host-derived factors released upon cell or tissue damage, such as uric acid, ATP, and hyaluronan (Schroder and Tschopp, 2010). NLRP6 assembly in the colonic epithelial compartment may be driven by a low level of these substances or by yet unidentified molecules signaling tissue integrity, resulting in local production of IL-18. Interestingly, in the rat, NLRP6, caspase-1, ASC, and pro-IL-18 are absent at embryonic day 16 (E16) and first appear at E20, with the processed form of IL-18 emerging in the gut during the early

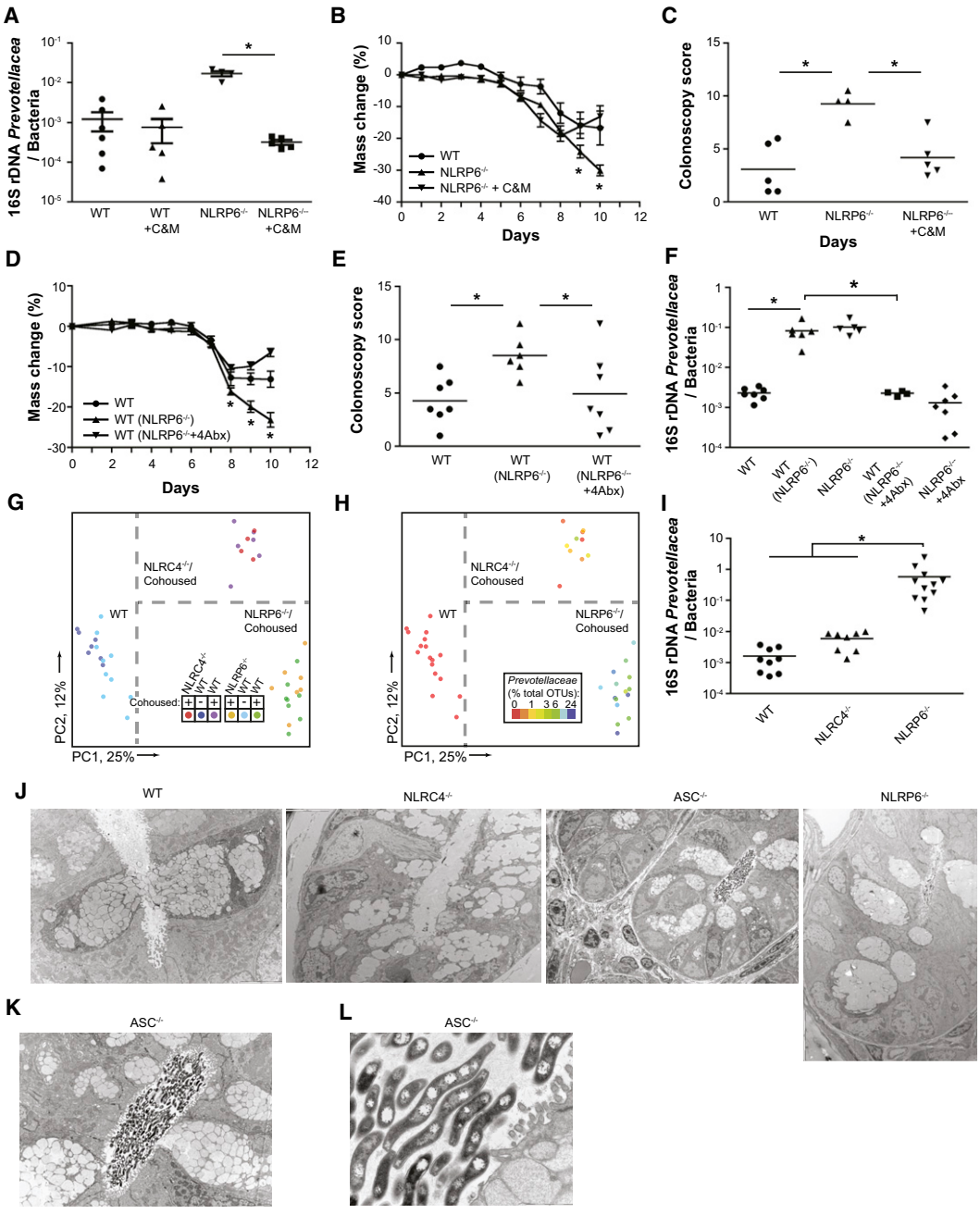

Figure 7. Decreased Abundance of Prevotella in Antibiotic-Treated *NLRP6*$^{-/-}$ Correlates with Ameliorated Colitogenic Microbiota

(A–C) WT and *NLRP6*$^{-/-}$ mice were treated with a combination of metronidazole and ciprofloxacin for 3 weeks. *Prevotellaceae* loads compared to total bacteria (A) were measured in fecal samples at the end of the antibiotic treatment period using qPCR analysis. DSS exposure was begun 3 days later. Weight loss (B) and colonoscopy score at day 7 (C).

(D–F) *NLRP6*$^{-/-}$ mice were treated with a combination of ampicillin, neomycin, vancomycin, and metronidazole for 3 weeks and then cohoused with WT mice for 4 weeks. In parallel, WT mice were cohoused with untreated *NLRP6*$^{-/-}$ mice. Subsequently, DSS colitis was induced, and weight (D) and colonoscopic assessments of mucosal damage at day 7 (E) were recorded. (F) qPCR assay for the abundance of Prevotella in fecal samples obtained after 4 weeks of cohousing.

(G and H) WT mice were cohoused for 4 weeks with either *NLRP6*$^{-/-}$ or *NLRC4*$^{-/-}$ mice. (G) Unweighted UniFrac PCoA of fecal microbiota harvested after cohousing. (H) Unweighted UniFrac PCoA colored by relative abundance of *Prevotellaceae* as percent of total OTUs.

(I) Quantification of *Prevotellaceae* in the crypt compartment, following extensive removal of stool content.

(J–L) Representative transmission electron microscopy images taken from colonic sections of WT (J, ×4200), *NLRC4*$^{-/-}$ (J, ×4200), *NLRP6*$^{-/-}$(J, ×2500), and *ASC*$^{-/-}$ mice (J, ×1700; K, ×4200; L, 26,000).

See Figure S6 for additional evidence linking bacterial components of the gut microbiota to the transmissible colonic inflammation in NLRP6 inflammasome-deficient mice.

postnatal period (Kempster et al., 2011), coinciding with the time of colonization of the gut ecosystem.

Dysbiosis may contribute to IBD by expansion of colitogenic strains such as entero-invasive *E.coli* (Darfeuille-Michaud et al., 2004), by reduction of tolerogenic strains such as *Faecalibacterium prausnitzi* (Sokol et al., 2008), or through a combination of both mechanisms. In our study, a colitogenic microbiota with altered representation of distinct bacterial members formed in the intestines of NLRP6-deficient mice; this microbiota was transferred across generations within a kinship and could displace the gut microbiota of cohoused immunocompetent mice. Once this community was horizontally transmitted to suckling or adult WT mice, it could persist. Compared to WT mice, NLRP6 inflammasome-deficient mice exhibit both quantitative and qualitative changes in numerous taxa, including increased representation of members of *Prevotellaceae* and TM7, and reductions in members of genus Lactobacillus in the Firmicutes phylum.

There are several intriguing links between the abundance of *Prevotellaceae* and TM7 and human diseases. *Prevotellaceae* has been implicated in periodontal disease (Kumar et al., 2003), and several reports have documented prominent representation of this group in samples from IBD patients (Kleessen et al., 2002; Lucke et al., 2006). *Prevetellaceae* might disrupt the mucosal barrier function through production of sulfatases that actively degrade mucus oligosaccharides (Wright et al., 2000); these enzymes are elevated in intestinal biopsies from IBD patients (Tsai et al., 1995). Though they have not been cultured, members of the TM7 phylum have been identified in 16S rRNA surveys of terrestrial and aquatic microbial communities as well in human periodontal disease (Brinig et al., 2003; Marcy et al., 2007; Ouverney et al., 2003) and in IBD patients (Kuehbacher et al., 2008). Defining the nature of the interactions of *Prevotellaceae* and TM7 with the NLRP6 inflammasome may provide insights about probiotic interventions that may mitigate microbiota-mediated enhanced inflammatory responses.

Four previous reports indicated that caspase-1, ASC, or NLRP3 deficiencies were associated with an increased severity of acute DSS colitis in mice and suggested that exacerbated disease was mediated, in part, by a defect in repair of the intestinal mucosa (Allen et al., 2010; Dupaul-Chicoine et al., 2010; Hirota et al., 2010; Zaki et al., 2010). Opposing results were found in two other studies using the same colitis model. The first study to investigate the role of caspase-1 in intestinal autoinflammation, even prior to the discovery of the inflammasome, found ameliorated acute and chronic colitis in *caspase-1*$^{-/-}$ mice (Siegmund et al., 2001). More recently, a second study demonstrated reduced severity of disease in *NLRP3*$^{-/-}$ mice that correlated with decreased levels of proinflammatory IL-1β (Bauer et al., 2010). It has been hypothesized that these differences might be the result of distinct roles of inflammasomes in nonhematopoietic versus hematopoietic cells (Siegmund, 2010). The proposed function in epithelial cells is to regulate secretion of IL-18 that stimulates epithelial cell barrier function and regeneration, whereas in hematopoietic cells, inflammasome activation would have a proinflammatory effect. Varying degrees of tissue injury and subsequent inflammation may result in shifting the balance between protective and detrimental effects, depending on the experimental condition and the inflammatory context. However, we believe that inflammasome-driven effects on the colonic microbiota, as revealed in our study, add yet another layer of regulation that affects and effects initiation of autoinflammation. As such, exacerbation in colitis severity in single-housed inflammasome-deficient mice may, in fact, involve defects in tissue regeneration, but this histopathological process may be dramatically influenced by the effects imposed by altered elements in the microbiota, including, for example, the enhanced representation of *Prevotellaceae* in the crypt. Thus, we propose that the fundamental role of the microbiota in shaping processes related to tissue damage, regeneration, and stress response might offer an explanation for the opposing results between these studies. 16S rRNA enumeration studies combined with various permutated cohousing experiments of the type described in this report, coupled with mechanistic molecular studies, would allow this notion to be tested directly. Furthermore, our results suggest that prolonged cohousing (or littermate controls) should be used when NLRs and other innate receptors are studied: this would allow for equilibration of differences in gut microbial ecology that may exist between groups of mice and allow investigators to determine which features of their phenotypes can be ascribed to the microbiota. Indeed, using cohousing conditions, we were able to demonstrate that the NLRC4 inflammasome is a direct negative regulator of colonic epithelial cell tumorigenesis that is not driven by the microbiota (Hu et al., 2010).

Our results show that the resultant aberrant microbiota promotes local epithelial induction of CCL5 transcription as a downstream mechanism, ultimately leading to an exaggerated autoinflammatory response. CCL5 is potently induced by bacterial and viral infections and, in turn, induces massive recruitment of a variety of innate and adaptive immune cells carrying CCR1, CCR3, CCR4, and CCR5 (Mantovani et al., 2004). Interestingly, both NOD2 and TLRs have been shown to induce CCL5 transcription (Bérubé et al., 2009; Werts et al., 2007). It will be of interest to investigate the crosstalk between these immune recognition systems in future experiments.

Recent studies have highlighted the importance of the gut microbiota in the pathogenesis of various autoimmune disorders that manifest outside of the gastrointestinal tract. In some autoimmune models, germ-free conditions or inoculation with a microbiota from healthy mice ameliorates disease (Lee et al., 2010; Mazmanian et al., 2008; Sinkorová et al., 2008; Wu et al., 2010). In contrast, rats with collagen-induced arthritis feature exacerbated disease when reared under germ-free conditions (Breban et al., 1993), whereas germ-free NOD *MyD88*$^{-/-}$ mice fail to develop diabetes, unlike their colonized counterparts (Wen et al., 2008). In humans, epidemiological evidence points to possible links between dysbiosis and rheumatoid arthritis, asthma, and atopic dermatitis (Björkstén, 1999; Penders et al., 2007; Vaahtovuo et al., 2008). Our study indicates that deficiencies in the NLRP6 pathway should be added to the list of host genetic factors that may drive disease-specific alterations in the microbiota, which in turn may promote disease in these hosts or in individuals who have been exposed to these microbial communities and who have also experienced disruption in their gut epithelial barrier function due to a variety of insults.

EXPERIMENTAL PROCEDURES

A detailed description of materials and methods used in this paper can be found in the Supplemental Information.

Mice

NLRP6$^{-/-}$ mice were generated by replacing exons 1 and 2 with a neomycin selection cassette (IRESnlslacZ/MC1neo). For cohousing experiments, age- and gender-matched WT and knockout mice were cohoused at 1:1 ratios for 4 weeks.

DSS Colitis

Mice were treated with 2% (w/v) DSS (M.W. = 36,000–50,000 Da; MP Biomedicals) in their drinking water for 7 days followed by regular access to water.

16S rRNA Analyses

Aliquots of frozen fecal samples (n = 211) were processed for DNA isolation using a previously validated protocol (Turnbaugh et al., 2009). ~365 bp amplicons, spanning variable region 2 (V2) of the 16S rRNA gene, were generated by using primer containing barcodes and sequenced on 454 sequencer. Data were processed using the QIIME (Quantitative Insights Into Microbial Ecology) analysis pipeline (Caporaso et al., 2010) and analyzed using UniFrac that defines the similarities and differences between microbial communities based on the degree to which community members share branch length on a bacterial tree of life (Lozupone and Knight, 2005).

Statistical Analysis

Data are expressed as mean ± SEM. Differences were analyzed by Student's t test and ANOVA and post-hoc analysis for multiple group comparison. p values $\leq$ 0.05 were considered significant.

Accession Numbers

16S rRNA data sets have been deposited in MG-RAST under accession number qiime:654.

SUPPLEMENTAL INFORMATION

Supplemental Information includes Extended Experimental Procedures, six figures, two data files, and one table and can be found with this article online at doi:10.1016/j.cell.2011.04.022.

ACKNOWLEDGMENTS

We would like to thank A Hafemann, S. Campton, E. Eynon, J. Alderman, W. Philbrick, C. Zorca, M. Musaheb, J. Stein, A. Ferrandino, F. Manzo, and the members of the Flavell lab for technical help and helpful discussions;K. Fitzgerald for providing *AIM2*$^{-/-}$ deficient mice; M. Graham and C. Rahner, CCMI EM Core Facility, Yale School of Medicine; J. Manchester and S. Deng for their assistance with DNA sequencing; V. Nagy for discussion and help with figure preparation; and H. Elinav for important discussions, suggestions, and critique. E.E. is supported by Cancer Research Institute (2010-2012) and the Israel-US educational foundation (2009) and is the recipient of the Claire and Emmanuel G. Rosenblatt award from the American Physicians for Medicine in Israel Foundation. A.L.K. is the recipient of a postdoctoral fellowship from the W.M Keck Foundation. J.H.-M. is supported by a LLS Postdoctoral Fellowship. This work was supported, in part, by Howard Hughes Medical Institute (R.A.F.) and the Crohn's and Colitis Foundation of America (J.I.G.).

Received: December 22, 2010
Revised: March 20, 2011
Accepted: April 22, 2011
Published online: May 12, 2011

REFERENCES

Agostini, L., Martinon, F., Burns, K., McDermott, M.F., Hawkins, P.N., and Tschopp, J. (2004). NALP3 forms an IL-1beta-processing inflammasome with increased activity in Muckle-Wells autoinflammatory disorder. Immunity *20*, 319–325.

Allen, I.C., TeKippe, E.M., Woodford, R.M., Uronis, J.M., Holl, E.K., Rogers, A.B., Herfarth, H.H., Jobin, C., and Ting, J.P. (2010). The NLRP3 inflammasome functions as a negative regulator of tumorigenesis during colitis-associated cancer. J. Exp. Med. *207*, 1045–1056.

Arthur, J.C., Lich, J.D., Ye, Z., Allen, I.C., Gris, D., Wilson, J.E., Schneider, M., Roney, K.E., O'Connor, B.P., Moore, C.B., et al. (2010). Cutting edge: NLRP12 controls dendritic and myeloid cell migration to affect contact hypersensitivity. J. Immunol. *185*, 4515–4519.

Bauer, C., Duewell, P., Mayer, C., Lehr, H.A., Fitzgerald, K.A., Dauer, M., Tschopp, J., Endres, S., Latz, E., and Schnurr, M. (2010). Colitis induced in mice with dextran sulfate sodium (DSS) is mediated by the NLRP3 inflammasome. Gut *59*, 1192–1199.

Becker, C., Fantini, M.C.,, and Neurath, M.F. (2006). High resolution colonoscopy in live mice. Nat. Protoc. *1*, 2900–2904.

Bérubé, J., Bourdon, C., Yao, Y., and Rousseau, S. (2009). Distinct intracellular signaling pathways control the synthesis of IL-8 and RANTES in TLR1/TLR2, TLR3 or NOD1 activated human airway epithelial cells. Cell. Signal. *21*, 448–456.

Björkstén, B. (1999). The environmental influence on childhood asthma. Allergy *54* (*Suppl 49*), 17–23.

Breban, M.A., Moreau, M.C., Fournier, C., Ducluzeau, R., and Kahn, M.F. (1993). Influence of the bacterial flora on collagen-induced arthritis in susceptible and resistant strains of rats. Clin. Exp. Rheumatol. *11*, 61–64.

Brinig, M.M., Lepp, P.W., Ouverney, C.C., Armitage, G.C., and Relman, D.A. (2003). Prevalence of bacteria of division TM7 in human subgingival plaque and their association with disease. Appl. Environ. Microbiol. *69*, 1687–1694.

Caporaso, J.G., Kuczynski, J., Stombaugh, J., Bittinger, K., Bushman, F.D., Costello, E.K., Fierer, N., Peña, A.G., Goodrich, J.K., Gordon, J.I., et al. (2010). QIIME allows analysis of high-throughput community sequencing data. Nat. Methods *7*, 335–336.

Darfeuille-Michaud, A., Boudeau, J., Bulois, P., Neut, C., Glasser, A.L., Barnich, N., Bringer, M.A., Swidsinski, A., Beaugerie, L., and Colombel, J.F. (2004). High prevalence of adherent-invasive Escherichia coli associated with ileal mucosa in Crohn's disease. Gastroenterology *127*, 412–421.

Dupaul-Chicoine, J., Yeretssian, G., Doiron, K., Bergstrom, K.S., McIntire, C.R., LeBlanc, P.M., Meunier, C., Turbide, C., Gros, P., Beauchemin, N., et al. (2010). Control of intestinal homeostasis, colitis, and colitis-associated colorectal cancer by the inflammatory caspases. Immunity *32*, 367–378.

Geijtenbeek, T.B., van Vliet, S.J., Engering, A., 't Hart, B.A., and van Kooyk, Y. (2004). Self- and nonself-recognition by C-type lectins on dendritic cells. Annu. Rev. Immunol. *22*, 33–54.

Grenier, J.M., Wang, L., Manji, G.A., Huang, W.J., Al-Garawi, A., Kelly, R., Carlson, A., Merriam, S., Lora, J.M., Briskin, M., et al. (2002). Functional screening of five PYPAF family members identifies PYPAF5 as a novel regulator of NF-kappaB and caspase-1. FEBS Lett. *530*, 73–78.

Hirota, S.A., Ng, J., Lueng, A., Khajah, M., Parhar, K., Li, Y., Lam, V., Potentier, M.S., Ng, K., Bawa, M., et al. (2010). NLRP3 inflammasome plays a key role in the regulation of intestinal homeostasis. Inflamm. Bowel Dis., in press. Published online September 24, 2010. 10.1002/ibd.21478.

Hu, B., Elinav, E., Huber, S., Booth, C.J., Strowig, T., Jin, C., Eisenbarth, S.C., and Flavell, R.A. (2010). Inflammation-induced tumorigenesis in the colon is regulated by caspase-1 and NLRC4. Proc. Natl. Acad. Sci. USA *107*, 21635–21640.

Hugenholtz, P., Tyson, G.W., Webb, R.I., Wagner, A.M., and Blackall, L.L. (2001). Investigation of candidate division TM7, a recently recognized major lineage of the domain Bacteria with no known pure-culture representatives. Appl. Environ. Microbiol. *67*, 411–419.

Janeway, C.A., Jr., and Medzhitov, R. (2002). Innate immune recognition. Annu. Rev. Immunol. *20*, 197–216.

Kempster, S.L., Belteki, G., Forhead, A.J., Fowden, A.L., Catalano, R.D., Lam, B.Y., McFarlane, I., Charnock-Jones, D.S., and Smith, G.C. (2011).

Developmental control of the Nlrp6 inflammasome and a substrate, IL-18, in mammalian intestine. Am. J. Physiol. Gastrointest. Liver Physiol. *300*, G253–G263.

Kleessen, B., Kroesen, A.J., Buhr, H.J., and Blaut, M. (2002). Mucosal and invading bacteria in patients with inflammatory bowel disease compared with controls. Scand. J. Gastroenterol. *37*, 1034–1041.

Kuehbacher, T., Rehman, A., Lepage, P., Hellmig, S., Fölsch, U.R., Schreiber, S., and Ott, S.J. (2008). Intestinal TM7 bacterial phylogenies in active inflammatory bowel disease. J. Med. Microbiol. *57*, 1569–1576.

Kufer, T.A., and Sansonetti, P.J. (2011). NLR functions beyond pathogen recognition. Nat. Immunol. *12*, 121–128.

Kumar, P.S., Griffen, A.L., Barton, J.A., Paster, B.J., Moeschberger, M.L., and Leys, E.J. (2003). New bacterial species associated with chronic periodontitis. J. Dent. Res. *82*, 338–344.

Lee, Y.K., Menezes, J.S., Umesaki, Y., and Mazmanian, S.K. (2010). Proinflammatory T-cell responses to gut microbiota promote experimental autoimmune encephalomyelitis. Proc. Natl. Acad. Sci. USA *108 Suppl 1*, 4615–4622.

Lozupone, C., and Knight, R. (2005). UniFrac: a new phylogenetic method for comparing microbial communities. Appl. Environ. Microbiol. *71*, 8228–8235.

Lucke, K., Miehlke, S., Jacobs, E., and Schuppler, M. (2006). Prevalence of Bacteroides and Prevotella spp. in ulcerative colitis. J. Med. Microbiol. *55*, 617–624.

Macpherson, A.J., and Uhr, T. (2004). Induction of protective IgA by intestinal dendritic cells carrying commensal bacteria. Science *303*, 1662–1665.

Mantovani, A., Sica, A., Sozzani, S., Allavena, P., Vecchi, A., and Locati, M. (2004). The chemokine system in diverse forms of macrophage activation and polarization. Trends Immunol. *25*, 677–686.

Marcy, Y., Ouverney, C., Bik, E.M., Lösekann, T., Ivanova, N., Martin, H.G., Szeto, E., Platt, D., Hugenholtz, P., Relman, D.A., and Quake, S.R. (2007). Dissecting biological "dark matter" with single-cell genetic analysis of rare and uncultivated TM7 microbes from the human mouth. Proc. Natl. Acad. Sci. USA *104*, 11889–11894.

Martinon, F., Burns, K., and Tschopp, J. (2002). The inflammasome: a molecular platform triggering activation of inflammatory caspases and processing of proIL-beta. Mol. Cell *10*, 417–426.

Matzinger, P. (2007). Friendly and dangerous signals: is the tissue in control? Nat. Immunol. *8*, 11–13.

Mazmanian, S.K., Round, J.L., and Kasper, D.L. (2008). A microbial symbiosis factor prevents intestinal inflammatory disease. Nature *453*, 620–625.

Niess, J.H., Brand, S., Gu, X., Landsman, L., Jung, S., McCormick, B.A., Vyas, J.M., Boes, M., Ploegh, H.L., Fox, J.G., et al. (2005). CX3CR1-mediated dendritic cell access to the intestinal lumen and bacterial clearance. Science *307*, 254–258.

Ouverney, C.C., Armitage, G.C., and Relman, D.A. (2003). Single-cell enumeration of an uncultivated TM7 subgroup in the human subgingival crevice. Appl. Environ. Microbiol. *69*, 6294–6298.

Penders, J., Stobberingh, E.E., van den Brandt, P.A., and Thijs, C. (2007). The role of the intestinal microbiota in the development of atopic disorders. Allergy *62*, 1223–1236.

Qin, J., Li, R., Raes, J., Arumugam, M., Burgdorf, K.S., Manichanh, C., Nielsen, T., Pons, N., Levenez, F., Yamada, T., et al; MetaHIT Consortium. (2010). A human gut microbial gene catalogue established by metagenomic sequencing. Nature *464*, 59–65.

Rakoff-Nahoum, S., Paglino, J., Eslami-Varzaneh, F., Edberg, S., and Medzhitov, R. (2004). Recognition of commensal microflora by toll-like receptors is required for intestinal homeostasis. Cell *118*, 229–241.

Rescigno, M., Urbano, M., Valzasina, B., Francolini, M., Rotta, G., Bonasio, R., Granucci, F., Kraehenbuhl, J.P., and Ricciardi-Castagnoli, P. (2001). Dendritic cells express tight junction proteins and penetrate gut epithelial monolayers to sample bacteria. Nat. Immunol. *2*, 361–367.

Schroder, K., and Tschopp, J. (2010). The inflammasomes. Cell *140*, 821–832.

Siegmund, B. (2010). Interleukin-18 in intestinal inflammation: friend and foe? Immunity *32*, 300–302.

Siegmund, B., Lehr, H.A., Fantuzzi, G., and Dinarello, C.A. (2001). IL-1 beta -converting enzyme (caspase-1) in intestinal inflammation. Proc. Natl. Acad. Sci. USA *98*, 13249–13254.

Sinkorová, Z., Capková, J., Niederlová, J., Stepánková, R., and Sinkora, J. (2008). Commensal intestinal bacterial strains trigger ankylosing enthesopathy of the ankle in inbred B10.BR (H-2(k)) male mice. Hum. Immunol. *69*, 845–850.

Sokol, H., Pigneur, B., Watterlot, L., Lakhdari, O., Bermúdez-Humarán, L.G., Gratadoux, J.J., Blugeon, S., Bridonneau, C., Furet, J.P., Corthier, G., et al. (2008). Faecalibacterium prausnitzii is an anti-inflammatory commensal bacterium identified by gut microbiota analysis of Crohn disease patients. Proc. Natl. Acad. Sci. USA *105*, 16731–16736.

Suzuki, K., Meek, B., Doi, Y., Muramatsu, M., Chiba, T., Honjo, T., and Fagarasan, S. (2004). Aberrant expansion of segmented filamentous bacteria in IgA-deficient gut. Proc. Natl. Acad. USA *101*, 1981–1986.

Tsai, H.H., Dwarakanath, A.D., Hart, C.A., Milton, J.D., and Rhodes, J.M. (1995). Increased faecal mucin sulphatase activity in ulcerative colitis: a potential target for treatment. Gut *36*, 570–576.

Turnbaugh, P.J., Hamady, M., Yatsunenko, T., Cantarel, B.L., Duncan, A., Ley, R.E., Sogin, M.L., Jones, W.J., Roe, B.A., Affourtit, J.P., et al. (2009). A core gut microbiome in obese and lean twins. Nature *457*, 480–484.

Vaahtovuo, J., Munukka, E., Korkeamäki, M., Luukkainen, R., and Toivanen, P. (2008). Fecal microbiota in early rheumatoid arthritis. J. Rheumatol. *35*, 1500–1505.

Vaishnava, S., Behrendt, C.L., Ismail, A.S., Eckmann, L., and Hooper, L.V. (2008). Paneth cells directly sense gut commensals and maintain homeostasis at the intestinal host-microbial interface. Proc. Natl. Acad. Sci. USA *105*, 20858–20863.

Wang, L., Manji, G.A., Grenier, J.M., Al-Garawi, A., Merriam, S., Lora, J.M., Geddes, B.J., Briskin, M., DiStefano, P.S., and Bertin, J. (2002). PYPAF7, a novel PYRIN-containing Apaf1-like protein that regulates activation of NF-kappa B and caspase-1-dependent cytokine processing. J. Biol. Chem. *277*, 29874–29880.

Wen, L., Ley, R.E., Volchkov, P.Y., Stranges, P.B., Avanesyan, L., Stonebraker, A.C., Hu, C., Wong, F.S., Szot, G.L., Bluestone, J.A., et al. (2008). Innate immunity and intestinal microbiota in the development of Type 1 diabetes. Nature *455*, 1109–1113.

Werts, C., le Bourhis, L., Liu, J., Magalhaes, J.G., Carneiro, L.A., Fritz, J.H., Stockinger, S., Balloy, V., Chignard, M., Decker, T., et al. (2007). Nod1 and Nod2 induce CCL5/RANTES through the NF-kappaB pathway. Eur. J. Immunol. *37*, 2499–2508.

Wright, D.P., Rosendale, D.I., and Robertson, A.M. (2000). Prevotella enzymes involved in mucin oligosaccharide degradation and evidence for a small operon of genes expressed during growth on mucin. FEMS Microbiol. Lett. *190*, 73–79.

Wu, H.J., Ivanov, I.I., Darce, J., Hattori, K., Shima, T., Umesaki, Y., Littman, D.R., Benoist, C., and Mathis, D. (2010). Gut-residing segmented filamentous bacteria drive autoimmune arthritis via T helper 17 cells. Immunity *32*, 815–827.

Zaki, M.H., Boyd, K.L., Vogel, P., Kastan, M.B., Lamkanfi, M., and Kanneganti, T.D. (2010). The NLRP3 inflammasome protects against loss of epithelial integrity and mortality during experimental colitis. Immunity *32*, 379–391.

Cell

EXTENDED EXPERIMENTAL PROCEDURES

Mice

NLRP6$^{-/-}$ mice were generated by replacing exons 1 and 2 with a neomycin selection cassette (IRESnlslacZ/MC1neo). *ASC*$^{-/-}$ (Pycard^{tm1Flv}(Sutterwala et al., 2006), *Casp1*$^{-/-}$ mice (Casp1^{tm1Flv}(Kuida et al., 1995), *NLRC4*$^{-/-}$ (Nlrc4^{tm1Gln}, (Lara-Tejero et al., 2006), all generated in our lab, *AIM2*$^{-/-}$ (Aim2$^{Gt(CSG445)Byg}$, (Rathinam et al., 2010), kindly provided by Dr. K Fitzgerald, University of Massachusetts), *NLRP12*$^{-/-}$ (Nlrp12^{tm1Jpyt}, (Arthur et al., 2010), obtained from Millenium Pharmaceuticals), *IL-18*$^{-/-}$ (Il18^{tm1Aki}, (Takeda et al., 1998), *IL-1R*$^{-/-}$ (Il1r1^{tm1Imx}, (Glaccum et al., 1997), both obtained from Jackson Laboratories, and *IL-1b*$^{-/-}$ mice (Il1b^{tm1Lvp}, kindly provided by Dr. G. Sebire, CHU de Sherbrooke, (Zheng et al., 1995) were described in previous publications. The generation of *NLRP10*$^{-/-}$ mice has not been published (S.C.E., unpublished data). *NLRP6*$^{-/-}$, *ASC*$^{-/-}$, *Casp1*$^{-/-}$, and *IL-18*$^{-/-}$ mice were backcrossed at least 10 times to C56Bl/6. *IL-1R*$^{-/-}$ mice were backcrossed five times to C56Bl/6, while *IL-1b*$^{-/-}$ mice were on a 129S7 background (and hence used for cohousing purposes only). WT C56Bl/6 mice were purchased from NCI. Where indicated, WT mice were also used that had been bred in our mouse barrier facility. All mice were specific pathogen-free, maintained under a strict 12h light cycle (lights on at 7:00am and off at 7:00pm), and given a regular chow diet (Harlan, diet #2018) *ad libitum.*

For cohousing experiments, age- and gender-matched WT and knockout mice were co-housed in new cages at 1:1 ratios for 4 weeks. For cross-fostering experiments, newborn mice were exchanged between *ASC*$^{-/-}$ and WT mothers within 24 hr of birth. Mice were weaned between postnatal days 21-28. For bone marrow chimera experiments, mice were given a sublethal dose of total body irradiation (2x 5.5 Gy, 3 hr apart). 16 hr later mice were transplanted with 4x10^6 unseparated bone marrow cells. Mice were analyzed 7-8 weeks later.

For antibiotic treatment, mice were given either (i) a combination of vancomycin (1 g/l), ampicilin (1 g/l), kanamycin (1 g/l), and metronidazole (1 g/l) or (ii) a combination of ciprofloxacin (0.2 g/l) and metronidazole (1 g/l) for 3 weeks in their drinking water. All antibiotics were obtained from Sigma Aldrich. All experimental procedures were approved by the local IACUC.

DSS Colitis

Mice were treated with 2% (w/v) DSS (M.W. = 36,000-50,000 Da; MP Biomedicals) in their drinking water for 7 days followed by regular access to water.

Colonoscopy

Colonoscopy was performed using a high resolution mouse video endoscopic system ('Coloview', Carl Storz, Tuttlingen, Germany). The severity of colitis was blindly scored using MEICS (Murine Endoscopic Index of Colitis Severity) which is based on five parameters: granularity of mucosal surface; vascular pattern; translucency of the colon mucosa; visible fibrin; and stool consistency (Becker et al., 2006).

Histology

Colons were fixed in Bouin's medium and embedded in paraffin. Blocks were serially sectioned along the cephalocaudal axis of the gut to the level of the lumen; the next 5 μm-thick section was stained with hematoxylin and eosin. Each section was scored by a pathologist who was blinded with respect to the origin of the sample: scoring was based on the degree of inflammation (location and extent), edema, mucosal ulceration, hyperplasia, crypt loss or abscess (Hu et al., 2010; O'Connor et al., 2009). Severity scores ranged from 0 to 5 with 0 being normal and 5 being most severe. Individual scores were assigned for each parameter, and then averaged for a final score per sample. Digital light microscopic images were recorded with a Zeiss Axio Imager.A1 microscope (Thornwood, NY), AxioCam MRc5 camera and AxioVision 4.7.1 imaging software (Carl Zeiss Microimaging). Results are displayed as percent involvement of colon (inflamed colon area) and by score of the most severe lesion in each sample (pathological severity score).

Immunofluorescence Staining

Frozen sections of colons from WT and *NLRP6*$^{-/-}$ mice were blocked in 10% fetal bovine serum for 1 hr at room temperature. Slides were incubated at 4°C for 16 hr with primary antibody to NLRP6 (clone E20, goat IgG, Santa Cruz Biotechnologies, Santa Cruz, California) at 2μg/ml, followed by incubation with 1:800 Alexa Fluor 647-labeled rabbit anti-goat secondary antibody (Invitrogen, Molecular Probes, Eugene Oregon) for 2 hr at 4°C. Sections were counterstained with 4,6-diamidino-2-phenylindole (DAPI) for nuclear staining. Slides were dried and mounted, using ProLong Antifade mounting medium (Invitrogen, Molecular Probes, Eugene Oregon). Slides were visualized using a Leica TCS SP5 confocal microscope.

Immunoprecipitation and Western Blot Analysis

Colons were excised and washed thoroughly by flushing several times with PBS, opened longitudinally, transferred into HBSS + 2 mM EDTA, and shaken for 20 min at 37°C. Subsequently, colons were washed 3 times with PBS and these washes were pooled with the HBSS fraction. This cell preparation containing a highly purified colonic epithelial cell fraction was spun down and resuspended in 1 ml / colon of ice-cold RIPA buffer containing protease inhibitors (Complete Mini EDTA-free, Roche). Cells were lysed

for 30 min at 4°C and lysates were spun for 30 min at maximum speed at 4°C using a tabletop centrifuge (Eppendorf). 500 μl of cleared lysates were immunoprecipated with 1 μg anti-NLRP6 antibody (clone E20, Santa Cruz Biotechnologies) and 25 μl of Protein G agarose (Invitrogen) for 12 hr at 4°C. Agarose beads were washed five times with RIPA buffer and finally bound proteins eluted by boiling in loading buffer. Samples were separated on 10% TGX gels (Biorad) and transferred onto PVDF membranes. Western blot analysis was performed using a anti-NLRP6 polyclonal antibody (clone E20, Santa Cruz Biotechnologies) and anti-Goat-HRP (Zymax).

Isolation of Colonic CD45$^+$ Cells and FACS Analysis and Sorting

Colons were excised and washed thoroughly by flushing several times with PBS. They were opened longitudinally, transferred into HBSS + 2 mM EDTA, and shaken for 20 min at 37C. Subsequently, colons were washed 3 times with PBS. The lamina propia was then digested for 45 min at 37°C using "digest solution" (DMEM containing 2% FCS, 2.5μg/ml Collagenase, 1 μg/ml DNaseI, and 1mM DTT). Single cell suspensions were obtained by grinding through a 100 μm cell strainer (Fisher Scientific). For FACS analysis, single suspensions were stained with anti-CD11c, anti-CD11b, anti-MHC class II, anti-TCR-beta, anti-TCR-gamma/delta, anti-B220, anti-NK1.1, and anti-CD45.2 (all from BD Biosciences or Biolegend) and analyzed on a BD LSR II. For FACS sorting, cells were stained with anti-mouse CD45.2-PacificBlue (Biolegend) and sorted twice iteratively on a BD FACS Aria to increase the purity of the positively sorted population.

Gene Expression Analysis

Tissues were preserved in RNAlater solution (Ambion) and subsequently homogenized in Trizol reagent (Invitrogen). Cells subjected to FACS were resuspended in Trizol reagent. RNA was purified according to the manufacturer's instructions. One microgram of total RNA was used to generate cDNA (HighCapacity cDNA Reverse Transcription kit; Applied Biosystems). RealTime-PCR was performed using gene-specific primer/probe sets (Applied Biosystems) and Kapa Probe Fast qPCR kit (Kapa Biosystems) on a 7500 Fast Real Time PCR instrument (Applied Biosystems). PCR conditions were 95°C for 20 s, followed by 40 cycles of 95°C for 3 s and 60°C for 30 s. Data were analyzed using the Sequence Detection Software according the deltaCt method with *hprt1* serving as the reference housekeeping gene.

Colonic Explants

Two 0.5 cm long pieces from the proximal colon were removed from a given animal, rinsed with PBS, and weighed. The tissue explants were cultured for 24 hr in DMEM medium containing 10% FBS, L-glutamine, penicillin, and streptomycin at 37°C. Culture medium was removed, centrifuged (1200 x g for 7 min at 4°C), and the resulting supernatant stored in aliquots at −20°C.

ELISA and Multiplex Analysis

Concentrations of cytokines and immunoglobulins in the serum or culture supernatants were measured using the following commercial ELISA kits: CCL5 (Peprotech); IL-18 (MBL); IgG1, IgG2c (BD Biosciences), IgA, IgM (Bethyl Laboratories) according to manufacturer's instruction. Multiplex analysis was performed using the Bioplex 23-Plex Panel (Biorad) according to the manufacturer's instructions.

16S rRNA Analyses

Aliquots of frozen fecal samples (n = 212) were processed for DNA isolation using a previously validated protocol (Turnbaugh et al., 2009). An aliquot of the purified fecal DNA was used for PCR amplification and sequencing of bacterial 16S rRNA genes. ~365bp amplicons, spanning variable region 2 (V2) of the 16S rRNA gene were generated by using (i) modified primer 8F (5′- CCATCTCA TCCCTGCGTGTCTCCGACTCAGTC*AGAGTTTGATCCTGGCTCAG*-3′) which consists of 454 Titanium primer B (underlined) and the universal bacterial primer 8F (italics) and (ii) modified primer 338R (5′ CCTATCCCCTGTGTGCCTTGGCAGTCTCAGNNNNNNNN CA*TGCTGCCTCCCGTAGGAGT* 3′) which contains 454 Titanium primer A (underlined), a sample specific, error correcting 8-mer barcode (N's), and the bacterial primer 338R (italics). Three replicate polymerase chain reactions were performed for each fecal DNA sample. The reactions were subsequently pooled, DNA was quantified (Picogreen), pooled in an equimolar ratio, purified (Ampure magnetic purification beads) and used for multiplex 454 pyrosequencing (Titanium chemistry). Reads were initially processed using the QIIME (Quantitative Insights Into Microbial Ecology) analysis pipeline (Caporaso et al., 2010): fasta, quality files and a mapping file indicating the barcode sequence corresponding to each sample were used as inputs. The QIIME pipeline takes this input information and splits reads by samples according to the barcode, performs taxonomical classification using the RDP-classifier, builds a *de-novo* taxonomic tree of the sequences based on sequence similarity, and creates a sample x OTUs table that can be used, together with the tree, for calculating beta diversity. After chimera removal, the dataset consisted of 747,125 sequences (average number of reads/fecal sample, 3,524 ± 1023 (SD); average read length, 361 nt). Sequences sharing ≥ 97% nucleotide sequence identity in the V2 region were binned into operation taxonomic units (97% ID OTUs) using uclust, chimeric sequences were removed using ChimeraSlayer (Haas et al., 2011). Note that we only considered 97% ID OTUs found 10 or more times among the 212 samples in our analyses. The OTU table was rarefied to 100 reads per sample to normalize the depth of sequencing per sample. (The OTU table used for our analyses is accessible at Data S1. A key describing the genotype and housing of each mouse (Table S1) shown in Figure 3 can be found at Data S2).

qPCR assays used previously reported primer pairs that target Prevotellaceae (5′-CCAGCCAAGTAGCGTGCA-3′ and 5′-TGGACCTTCCGTATTACC-3′) (Dalwai et al., 2007), TM7 (5′-GCAACTCTTTACGCCCAGT-3′ and 5′-GAGAGGATGATCAGCCAG-3′) and Bacteria (5′-AGAGTTTGATCCTGGCTC-3′ and 5′-TGCTGCCTCCCGTAGGAGT-3′) (Björsdorff et al., 2002). The PCR mix contained 5 μl of the sample DNA solution, 5 pmol of each primer, 0.2 μl of bacteria-specific probes and 5 μl of Universal qPCR mix (Kapa Biosystems, Boston, USA). PCR conditions were 95°C for 120 s, followed by 40 cycles of 95°C for 3 s and 64°C for 30 s. Data were analyzed using the Sequence Detection Software according the deltaCt method by normalizing tested bacterial species to total bacteria for each sample.

To quantify attached bacteria enriched in the crypts, colons were excised and thoroughly washed five times with 10 ml of PBS to remove all fecal contents. Tissues were then homogenized in Trizol and genomic DNA was purified according to the manufacturer's instructions.

Statistical Analysis

Data are expressed as mean ± SEM. Differences were analyzed by Student's t test and ANOVA, and post-hoc analysis for multiple group comparison. p values ≤ 0.05 were considered significant.

SUPPLEMENTAL REFERENCES

Arthur, J.C., Lich, J.D., Ye, Z., Allen, I.C., Gris, D., Wilson, J.E., Schneider, M., Roney, K.E., O'Connor, B.P., Moore, C.B., et al. (2010). Cutting edge: NLRP12 controls dendritic and myeloid cell migration to affect contact hypersensitivity. J. Immunol. *185*, 4515–4519.

Björsdorff, A., Bagert, B., Massung, R.F., Gusa, A., and Eliasson, I. (2002). Isolation and characterization of two European strains of Ehrlichia phagocytophila of equine origin. Clin. Diagn. Lab. Immunol. *9*, 341–343.

Caporaso, J.G., Kuczynski, J., Stombaugh, J., Bittinger, K., Bushman, F.D., Costello, E.K., Fierer, N., Peña, A.G., Goodrich, J.K., Gordon, J.I., et al. (2010). QIIME allows analysis of high-throughput community sequencing data. Nat. Methods *7*, 335–336.

Dalwai, F., Spratt, D.A., and Pratten, J. (2007). Use of quantitative PCR and culture methods to characterize ecological flux in bacterial biofilms. J. Clin. Microbiol. *45*, 3072–3076.

Glaccum, M.B., Stocking, K.L., Charrier, K., Smith, J.L., Willis, C.R., Maliszewski, C., Livingston, D.J., Peschon, J.J., and Morrissey, P.J. (1997). Phenotypic and functional characterization of mice that lack the type I receptor for IL-1. J. Immunol. *159*, 3364–3371.

Haas, B.J., Gevers, D., Earl, A.M., Feldgarden, M., Ward, D.V., Giannoukos, G., Ciulla, D., Tabbaa, D., Highlander, S.K., Sodergren, E., et al; Human Microbiome Consortium. (2011). Chimeric 16S rRNA sequence formation and detection in Sanger and 454-pyrosequenced PCR amplicons. Genome Res. *21*, 494–504.

Hu, B., Elinav, E., Huber, S., Booth, C.J., Strowig, T., Jin, C., Eisenbarth, S.C., and Flavell, R.A. (2010). Inflammation-induced tumorigenesis in the colon is regulated by caspase-1 and NLRC4. Proc. Natl. Acad. Sci. USA *107*, 21635–21640.

Kuida, K., Lippke, J.A., Ku, G., Harding, M.W., Livingston, D.J., Su, M.S., and Flavell, R.A. (1995). Altered cytokine export and apoptosis in mice deficient in interleukin-1 beta converting enzyme. Science *267*, 2000–2003.

Lara-Tejero, M., Sutterwala, F.S., Ogura, Y., Grant, E.P., Bertin, J., Coyle, A.J., Flavell, R.A., and Galán, J.E. (2006). Role of the caspase-1 inflammasome in Salmonella typhimurium pathogenesis. J. Exp. Med. *203*, 1407–1412.

O'Connor, W., Jr., Kamanaka, M., Booth, C.J., Town, T., Nakae, S., Iwakura, Y., Kolls, J.K., and Flavell, R.A. (2009). A protective function for interleukin 17A in T cell-mediated intestinal inflammation. Nat. Immunol. *10*, 603–609.

Rathinam, V.A., Jiang, Z., Waggoner, S.N., Sharma, S., Cole, L.E., Waggoner, L., Vanaja, S.K., Monks, B.G., Ganesan, S., Latz, E., et al. (2010). The AIM2 inflammasome is essential for host defense against cytosolic bacteria and DNA viruses. Nat. Immunol. *11*, 395–402.

Sutterwala, F.S., Ogura, Y., Szczepanik, M., Lara-Tejero, M., Lichtenberger, G.S., Grant, E.P., Bertin, J., Coyle, A.J., Galán, J.E., Askenase, P.W., and Flavell, R.A. (2006). Critical role for NALP3/CIAS1/Cryopyrin in innate and adaptive immunity through its regulation of caspase-1. Immunity *24*, 317–327.

Takeda, K., Tsutsui, H., Yoshimoto, T., Adachi, O., Yoshida, N., Kishimoto, T., Okamura, H., Nakanishi, K., and Akira, S. (1998). Defective NK cell activity and Th1 response in IL-18-deficient mice. Immunity *8*, 383–390.

Turnbaugh, P.J., Hamady, M., Yatsunenko, T., Cantarel, B.L., Duncan, A., Ley, R.E., Sogin, M.L., Jones, W.J., Roe, B.A., Affourtit, J.P., et al. (2009). A core gut microbiome in obese and lean twins. Nature *457*, 480–484.

Zheng, H., Fletcher, D., Kozak, W., Jiang, M., Hofmann, K.J., Conn, C.A., Soszynski, D., Grabiec, C., Trumbauer, M.E., Shaw, A., et al. (1995). Resistance to fever induction and impaired acute-phase response in interleukin-1 beta-deficient mice. Immunity *3*, 9–19.

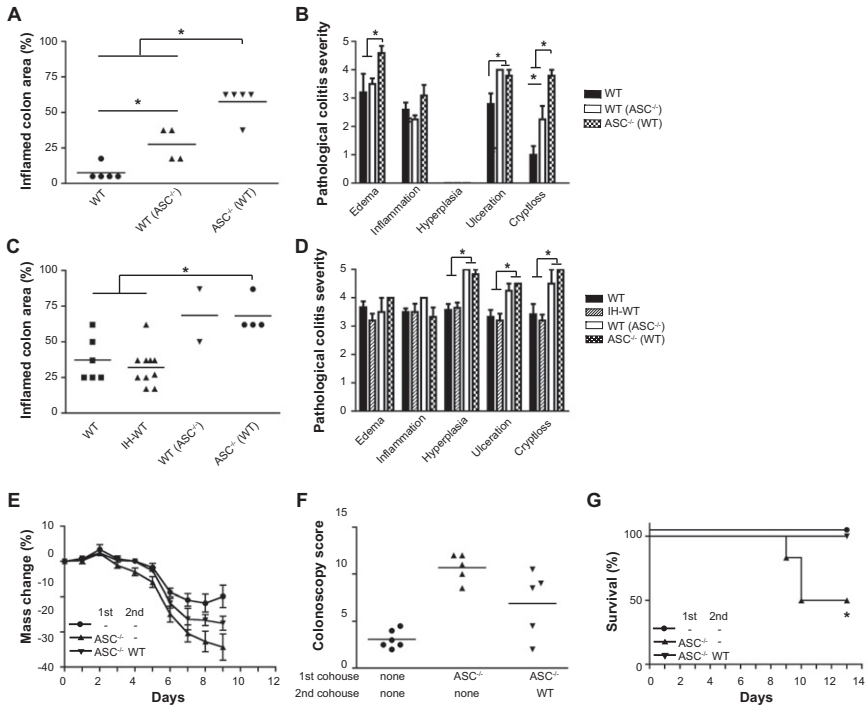

Figure S1. Increased Tissue Damage in *ASC*$^{-/-}$ Mice and in WT Mice Cohoused with *ASC*$^{-/-}$ Mice, Related to Figure 1 and Figure 2

(A–D) Quantification of the histological severity of DSS colitis in single-housed WT mice, cohoused WT mice, and *ASC*$^{-/-}$ mice on day 6 (A and B) and on day 12 (C and D) after initiation of treatment. In (A and B) WT mice are compared to WT and *ASC*$^{-/-}$ mice cohoused with each other ((WT(*ASC*$^{-/-}$) and *ASC*$^{-/-}$(WT), respectively)). In (C, D) WT mice are compared to in-house bred WT mice (IH-WT), and WT and ASC$^{-/-}$ mice cohoused with each other ((WT(*ASC*$^{-/-}$) and *ASC*$^{-/-}$(WT), respectively)). Results were calculated as the percentage of inflamed colon area (A, C), and the pathological colitis severity scored in the worst affected area (B, D), as quantified by the parameters inflammation, edema, ulceration, hyperplasia and crypt loss. Each parameter was scored by a pathologist, who was blinded to genotype or treatment, between 0 (normal) to 5 (severe).

(E–G) WT mice were cohoused or not cohoused in two steps to evaluate the stability of the altered flora in WT mice. They were either never cohoused (1st none, 2nd none), cohoused for 4 weeks with *ASC*$^{-/-}$ mice and then housed separately for 4 weeks (1st *ASC*$^{-/-}$, 2nd none), or after their cohousing with *ASC*$^{-/-}$ mice cohoused with a new cohort of WT mice (1st *ASC*$^{-/-}$, 2nd WT). DSS colitis was induced subsequently in these mice and body weight (E), colonoscopy score at day 7 (F) and survival (G) were monitored; * denotes significance of $p < 0.05$ by One-way ANOVA.

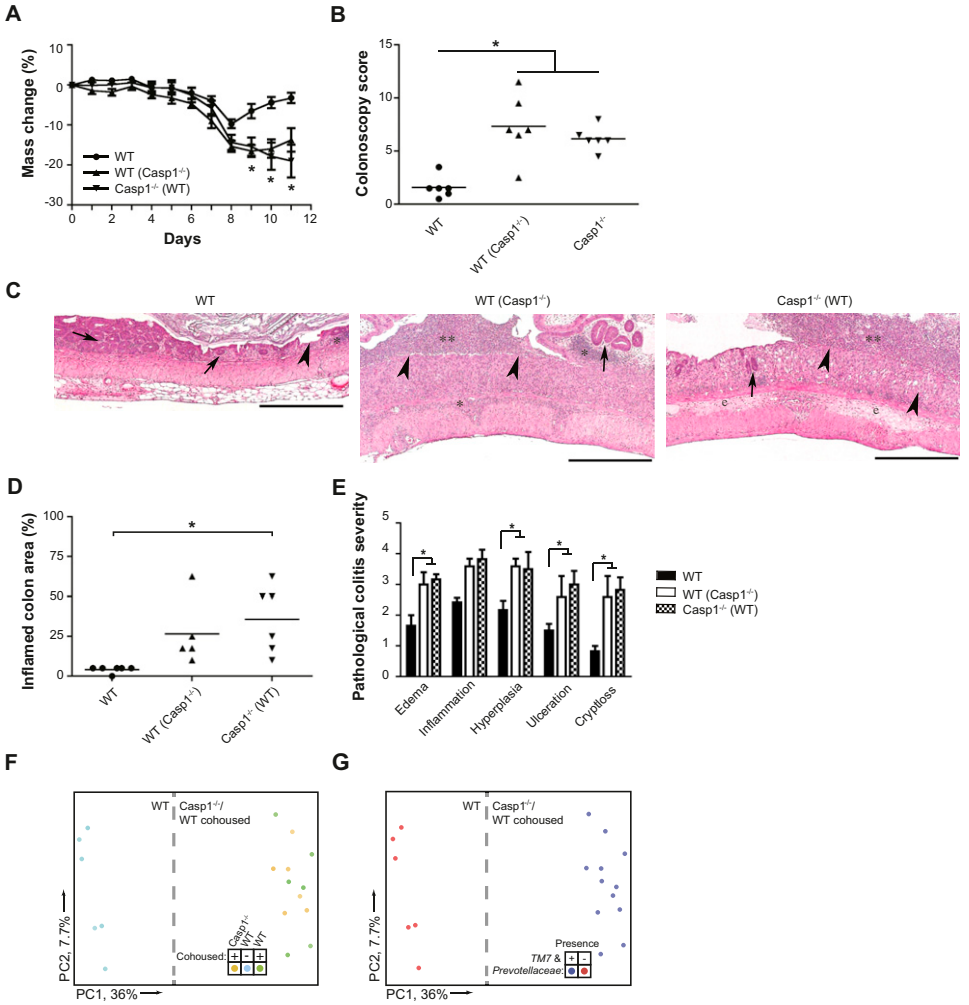

Figure S2. Exacerbated Colitis Severity in Caspase-1-Deficent Mice Is Transmissible to Cohoused Wild-Type Mice, Related to Figure 3

(A–E) DSS colitis was induced in single-housed WT mice as well as in WT mice cohoused with *Casp1*$^{-/-}$ mice (WT(*Casp1*$^{-/-}$) and Casp1$^{-/-}$(WT), respectively). Weight (A), colonoscopy score at day 7 (B), and histological severity of colitis at day 12 (C-E) were compared. (C) Representative hematoxylin and eosin-stained sections of colons from single-housed WT mice, WT mice cohoused with Casp1$^{-/-}$ mice, and *Casp1*$^{-/-}$ mice cohoused with WT mice. Colons from *Casp1*$^{-/-}$ mice and WT mice cohoused with *Casp1*$^{-/-}$ mice both feature severe pathologic changes, as evidenced by marked epithelial ulceration (arrowheads), loss of crypts, and severe edema (e) /inflammation (*) and flooding of the lumen with inflammatory cells (**). In contrast, colons from WT single house mice had smaller and fewer foci of ulceration (arrowhead), with retention/regeneration of crypts (arrows). Scale bars = 500 μm. (D, E) Results were calculated as the percentage of inflamed colon area (D), and the pathological colitis severity scored in the worst affected area (E), as quantified by the parameters inflammation, edema, ulceration, hyperplasia and crypt loss. Each parameter was scored by a blinded pathologist between 0 (normal) to 5 (severe).

(F) Unweighted UniFrac PCoA of fecal microbiota harvested from untreated WT mice single-housed or co-housed with *Casp1*$^{-/-}$ mice.

(G) Unweighted UniFrac PCoA demonstrating presence or absence of TM7 and Prevotellaceae in each sample (color key provided at the lower right of the panel). Dashed lines show separation of single-housed WT and co-housed WT and knockout mice on PC1. * represents significance of $p < 0.05$ by One-way ANOVA.

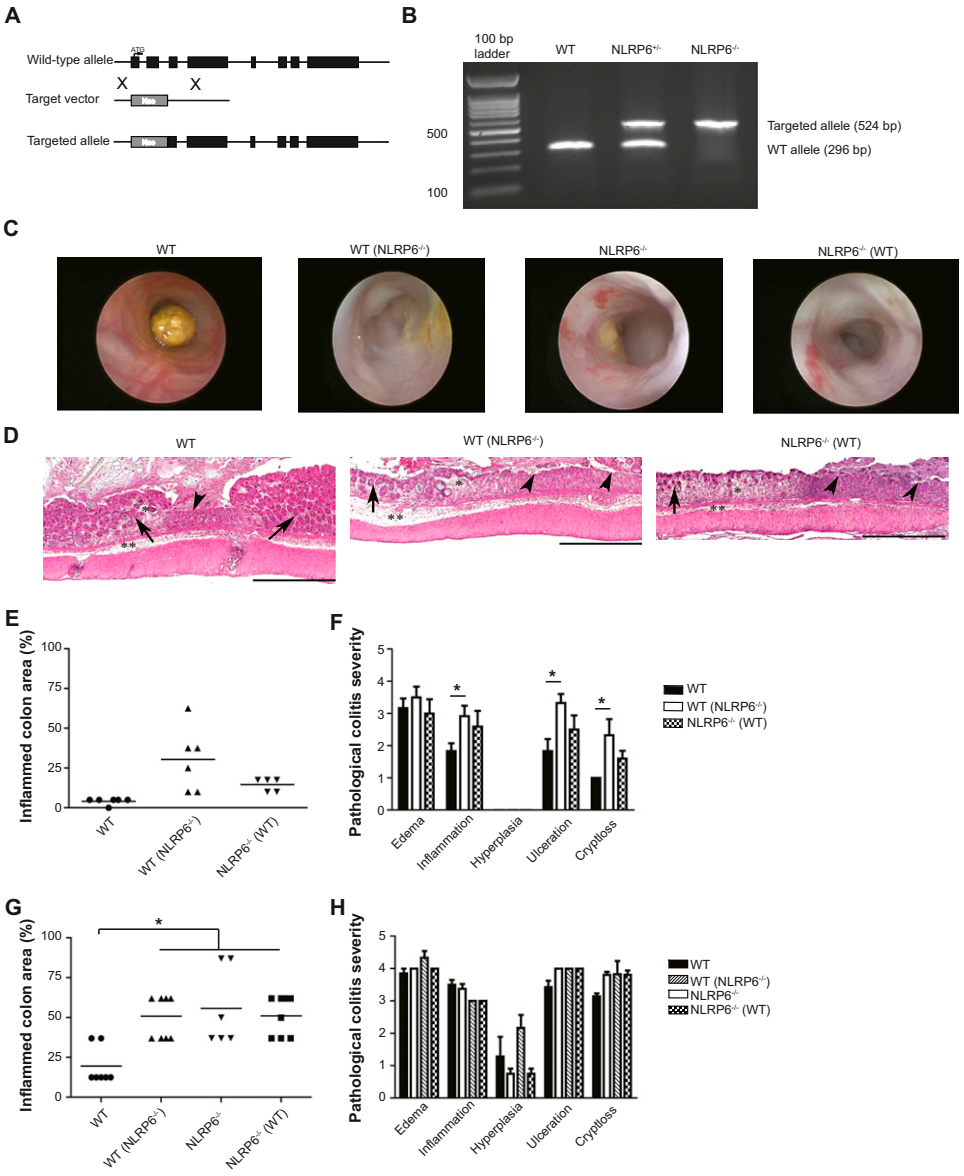

Figure S3. Increased Tissue Damage in *NLRP6*$^{-/-}$ Mice and in WT Mice Cohoused with *NLRP6*$^{-/-}$ Mice, Related to Figure 4

(A) NLRP6-deficient mice were generated by replacing Exons 1 and 2 with a neomycin resistance cassette resulting in a truncated gene that lacks the ATG and the coding region for the pyrin domain.

(B) PCR screening strategy for deletion of NLRP6. WT allele 296 bp, targeted allele 524 bp.

(C) Representative images of the colonic mucosa taken during colonoscopy on day 8 of DSS colitis.

(D) Representative hematoxylin and eosin-stained sections of colons from WT (WT), WT(*NLRP6*$^{-/-}$) and *NLRP6*$^{-/-}$(WT) mice sampled on day 6 after induction of DSS colitis. The predominant early differences are evidenced by marked epithelial ulceration (arrowheads), greater loss of crypts, and edema not not only within the submucosa (**), but also within the lamina propria (*). In contrast, colons from WT single house mice had smaller and significantly fewer foci of ulceration (arrowhead), with retention of crypts (arrows). Scale bars = 500 μm.

(E–H) Quantification of the histological colitis severity in single-housed WT mice (WT), in WT mice cohoused for 4 weeks with *NLRP6*$^{-/-}$ mice (WT(*NLRP6*$^{-/-}$)), the corresponding co-housed *NLRP6*$^{-/-}$ mice (*NLRP6*$^{-/-}$(WT)) and single-housed *NLRP6*$^{-/-}$ mice (*NLRP6*$^{-/-}$) on day 6 (E-F) and on day 8 (G, H) after induction of DSS colitis. Results were calculated as the percentage of inflamed colon area (E, G), and the pathological colitis severity (F, H), as quantified by the parameters inflammation, edema, ulceration, hyperplasia and crypt loss. Each parameter was scored by a blinded pathologist between 0 (normal) to 5 (severe); * represents significance of $p < 0.05$ by One-way ANOVA.

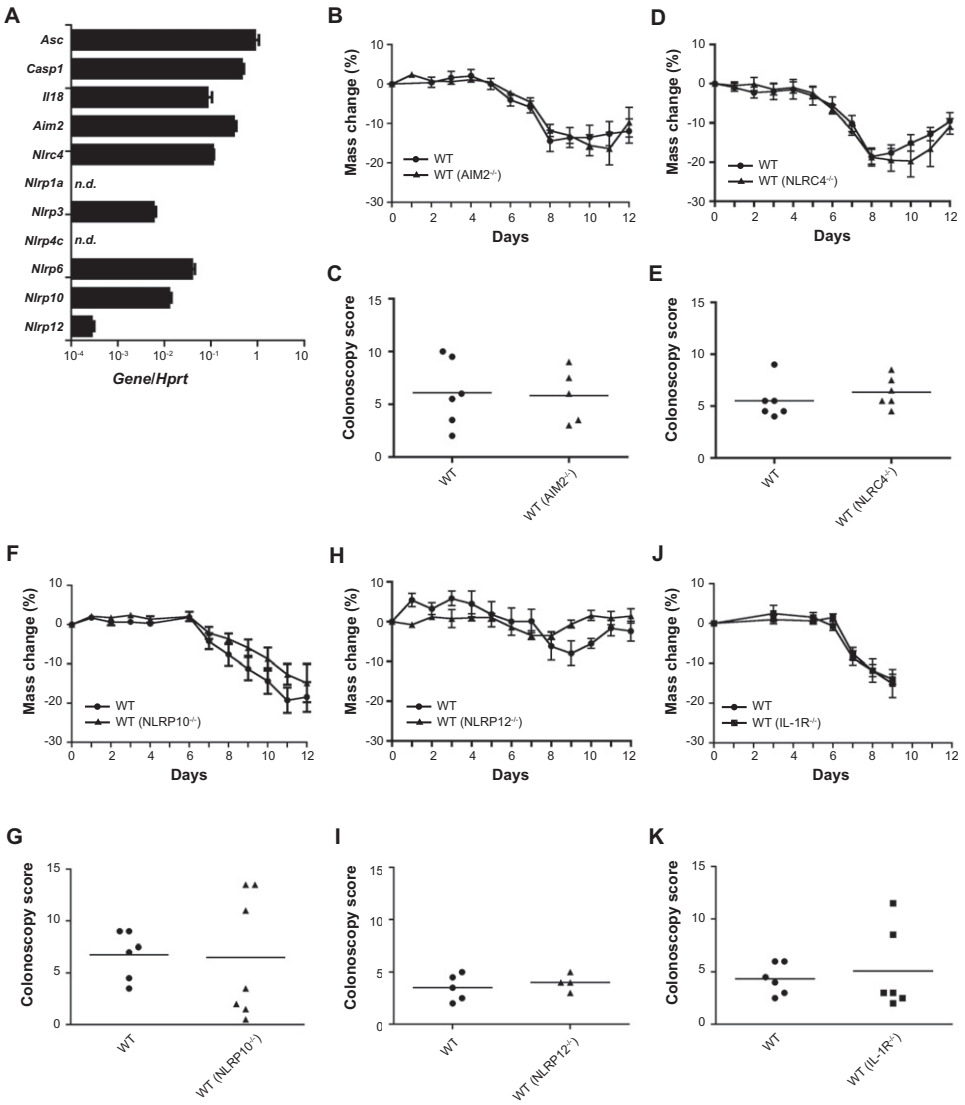

Figure S4. Other NLR-Deficient and Inflammasome-Associated Mouse Strains Do Not House a Colitogenic Transmissible Microbiota, Related to Figure 5

(A) qRT-PCR analysis of the expression of inflammasome-associated genes as well as several NLR genes in total colonic RNA, n.d. not detectable.

(B–K) WT mice were cohoused for 4 weeks with (B, C) *AIM2*$^{-/-}$ mice, (D, E) *NLRC4*$^{-/-}$ mice, (F, G) *NLRP10*$^{-/-}$ mice, (H, I) *NLRP12*$^{-/-}$ mice and (J, K) *IL-1R*$^{-/-}$ mice and subsequently colitis was induced by treatment with DSS. Weight loss (B, D, F, H, and J) and colonoscopy score (C, E, G, I, and K) were compared between single-housed and cohoused WT mice.

Data are representative of at least two independent experiments. Error bars represent the SEM of samples within a group.

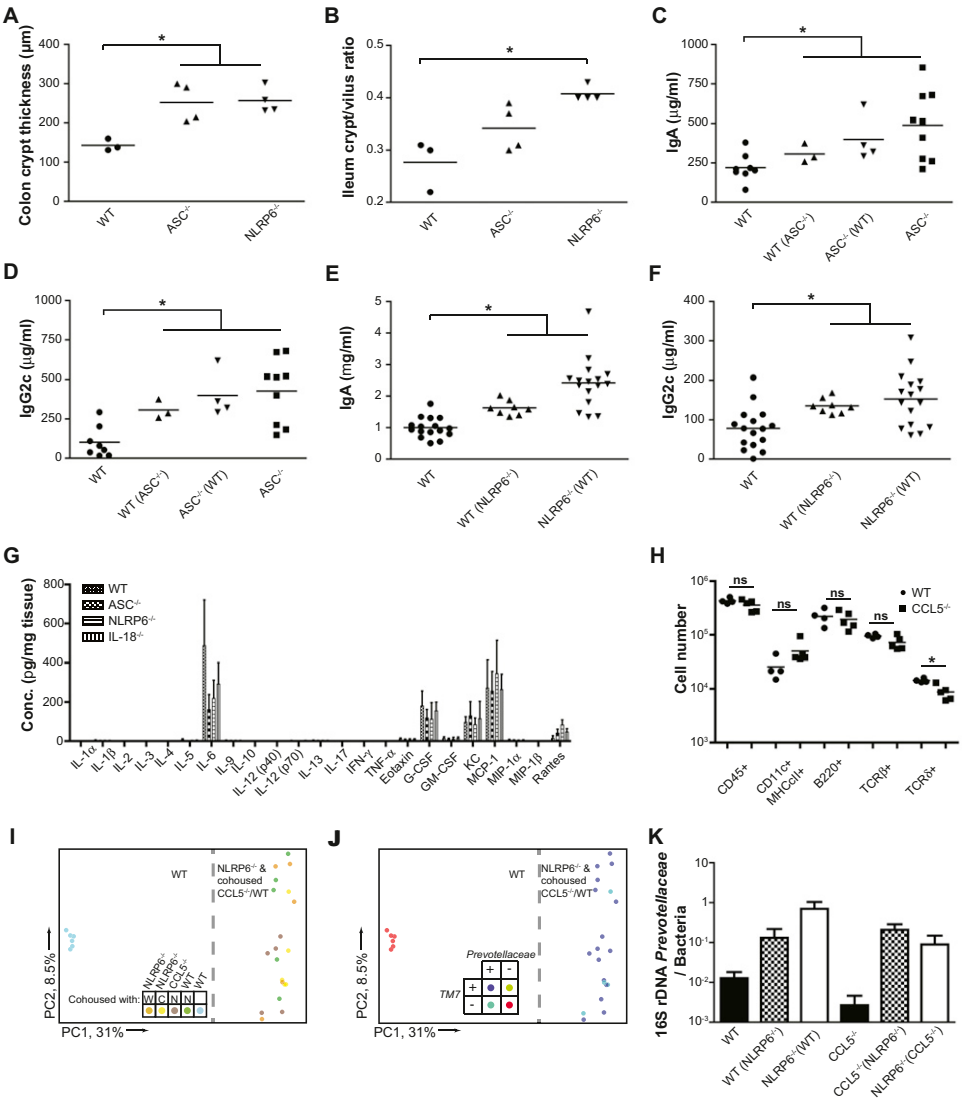

Figure S5. CCL5 Is Essential for the Development of Exacerbated Colitis in Cohoused WT Mice, Related to Figure 6

(A and B) Quantification of spontaneous hyperplasia in *ASC*$^{-/-}$ and *NLRP6*$^{-/-}$ mice compared to WT mice.

(C–F) Levels of total IgG2c and IgA levels were measured in the serum of (C, D) single-housed and cohoused WT and ASC mice as well as (E, F) *NLRP6*$^{-/-}$ mice, respectively. Data are pooled data from 2 independent experiments.

(G) Multiplex analysis of cytokine and chemokine production in colon tissue explants.

(H) Quantification of total lamina propria immune cells (CD45^{+}) and immune cell subsets (Dendritic cells, B cells, αβ T cells, and γδ T cells) in WT and CCL5$^{-/-}$ mice in the steady state.

(I) Unweighted UniFrac PCoA of fecal microbiota harvested from untreated WT and CCL5$^{-/-}$ mice single-housed or co-housed with NLRP6$^{-/-}$ mice.

(J) Unweighted UniFrac PCoA demonstrating presence or absence of TM7 and *Prevotellaceae* in each sample (color key provided at the lower left of the panel). Dashed lines show separation of single-housed and co-housed WT and knockout mice on PC1.

(K) Quantification of *Prevotellaceae* 16S rDNA copy numbers normalized to total bacteria. *represents $p < 0.05$ by One-way ANOVA. ns = non significant.

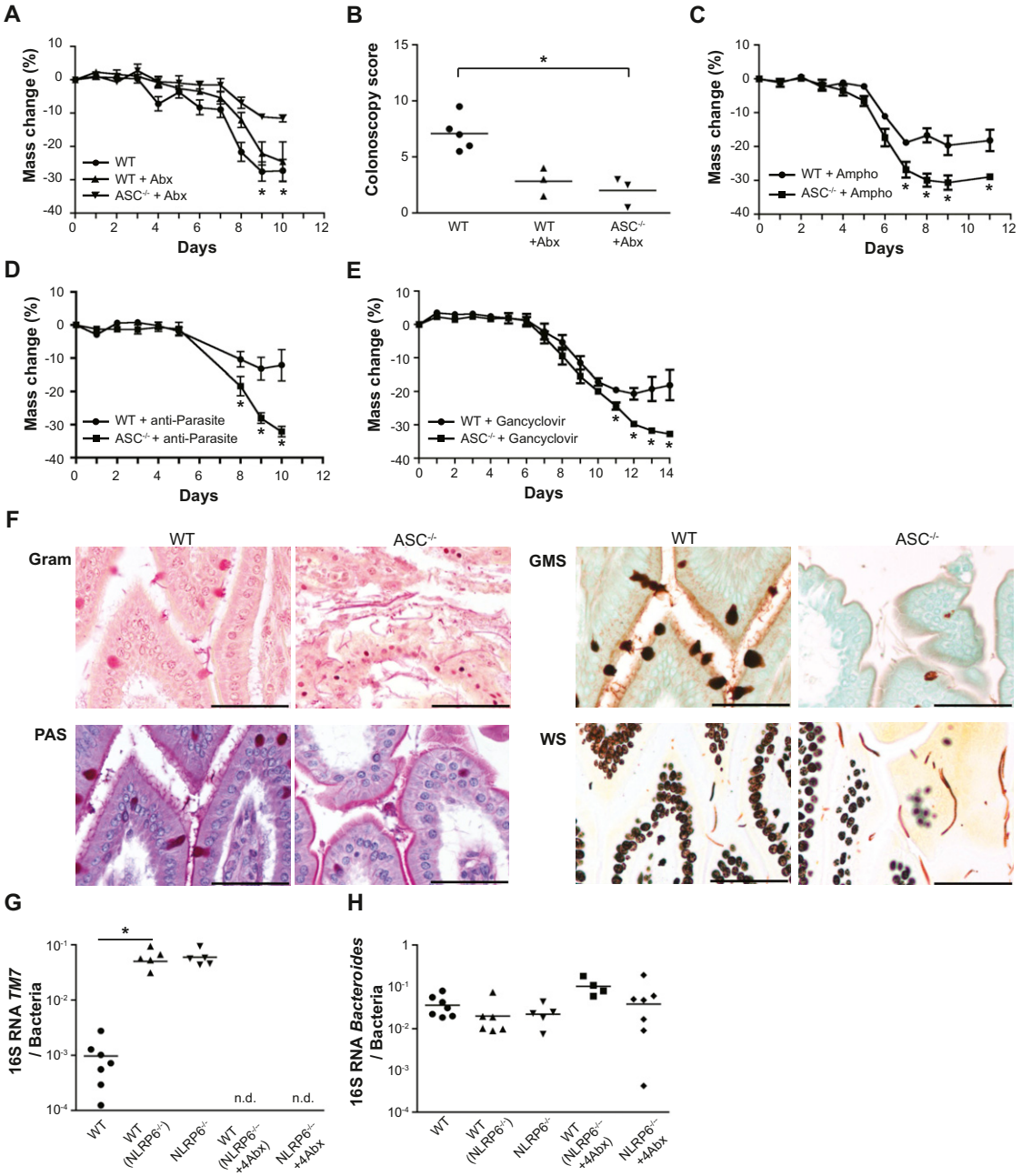

Figure S6. The More Severe DSS-Induced Colitis in ASC-Deficient Compared to WT Mice Is Ameliorated with Broad-Spectrum Antibacterial Treatment, but Not Treatment with Amphotericin B, Gancyclovir, or Albendazole and Praziquantel, Related to Figure 7

(A and B) WT and *ASC*$^{-/-}$ mice were treated orally with metronidazole/ciprofloxacin for 3 weeks and colitis was induced subsequently. (A) Changes in body weight and (B) colonoscopy score were compared.

(C–E) *ASC*$^{-/-}$ mice were treated for the indicated time intervals with (C) amphotericin B (anti-fungal, 3 weeks), (D) albendazole and praziquantel (anti-parasitic, 2 weeks) or (E) gancyclovir (anti-herpesvirus, 2 weeks). Subsequently, colitis was induced and weight loss was compared. Error bars represent the SEM of samples within a treatment group.

(F) Representative sections of terminal ileum stained with hematoxylin and eosin (HE), Gram, Geimsa (GMS), and Warthin-Starry (WS) stains reveal numerous long striated, Gram-negative, GMS-negative, WS-positive rod-shaped bacteria in *ASC*$^{-/-}$mice and few in WT mice. Scale bars - 50 μm.

(G and H) *NLRP6*$^{-/-}$ mice were treated with a combination of ampicillin, neomycin, vancomycin, and metronidazole for 3 weeks and then co-housed with WT mice for 4 weeks. In parallel, WT mice were co-housed with untreated *NLRP6*$^{-/-}$ mice. qPCR assay for the abundance of TM7 (G), and Bacteroides (H) in fecal samples obtained after 4 weeks of cohousing.